

INFORMATION TO USERS

This manuscript has been reproduced from the microfilm master. UMI films the text directly from the original or copy submitted. Thus, some thesis and dissertation copies are in typewriter face, while others may be from any type of computer printer.

The quality of this reproduction is dependent upon the quality of the copy submitted. Broken or indistinct print, colored or poor quality illustrations and photographs, print bleedthrough, substandard margins, and improper alignment can adversely affect reproduction.

In the unlikely event that the author did not send UMI a complete manuscript and there are missing pages, these will be noted. Also, if unauthorized copyright material had to be removed, a note will indicate the deletion.

Oversize materials (e.g., maps, drawings, charts) are reproduced by sectioning the original, beginning at the upper left-hand corner and continuing from left to right in equal sections with small overlaps.

Photographs included in the original manuscript have been reproduced xerographically in this copy. Higher quality 6" x 9" black and white photographic prints are available for any photographs or illustrations appearing in this copy for an additional charge. Contact UMI directly to order.

ProQuest Information and Learning
300 North Zeeb Road, Ann Arbor, MI 48106-1346 USA
800-521-0600

UMI[®]

INFLUENCE OF SIZE ON PUNCHING SHEAR STRENGTH OF CONCRETE SLABS

by

Kevin Ka Lun Li

March 2000



Department of Civil Engineering and Applied Mechanics

McGill University

Montreal, Canada

**A thesis submitted to the Faculty of Graduate Studies
and Research in partial fulfilment of the requirements
for the degree of Master of Engineering**

© Kevin Ka Lun Li, 2000



National Library
of Canada

Acquisitions and
Bibliographic Services

395 Wellington Street
Ottawa ON K1A 0N4
Canada

Bibliothèque nationale
du Canada

Acquisitions et
services bibliographiques

395, rue Wellington
Ottawa ON K1A 0N4
Canada

Your file *Votre référence*

Our file *Notre référence*

The author has granted a non-exclusive licence allowing the National Library of Canada to reproduce, loan, distribute or sell copies of this thesis in microform, paper or electronic formats.

The author retains ownership of the copyright in this thesis. Neither the thesis nor substantial extracts from it may be printed or otherwise reproduced without the author's permission.

L'auteur a accordé une licence non exclusive permettant à la Bibliothèque nationale du Canada de reproduire, prêter, distribuer ou vendre des copies de cette thèse sous la forme de microfiche/film, de reproduction sur papier ou sur format électronique.

L'auteur conserve la propriété du droit d'auteur qui protège cette thèse. Ni la thèse ni des extraits substantiels de celle-ci ne doivent être imprimés ou autrement reproduits sans son autorisation.

0-612-64235-6

Canada

To My Parents

Influence of Size on Punching Shear Strength of Concrete Slabs

Abstract

The punching shear behaviour of interior slab-column connections in flat plates is investigated. The response of six two-way slab specimens, which were designed such that they would fail in punching shear, are presented. The parameter introduced in the experimental program is member depth. The effects of this parameter on the punching shear capacity of slab elements are investigated. The results show a strong "size effect" with deeper members having a smaller shear stresses at failure than shallow ones.

Test results obtained from this experimental program are compared with the punching shear predictions of the Canadian CSA A23.3-94 Standard, the American ACI 318-95 Code, the British BS 8110-85 Standard and the European CEB-FIP 1990 Model Code. Predictions were also made using computer program "Response 2000", assuming an equivalent beam analogy to represent the slab. It is concluded that the shear design of slabs, according to the current Canadian and American codes, can be unconservative under certain conditions, particularly for thick slabs. It is recommended that the punching shear expressions of the CSA Standard and the ACI Code be modified to take into account the "size effect" on the punching shear strength of slabs.

Résumé

L'auteur étudie le poinçonnement des dalles armées dans les deux directions principales au droit des joints dalle-colonnes, à l'aide de six sous-assemblages dalle-colonne testés en laboratoire. Le paramètre étudié dans le programme d'essais est l'épaisseur de la dalle. Les résultats d'essais indiquent un effet d'échelle important, les dalles les plus épaisses présentant des contraintes de cisaillement à la rupture inférieures à celles des dalles plus minces.

Ces résultats expérimentaux ont également été comparés aux prédictions des normes canadienne CSA A23.3-94, américaine ACI 318-95, britannique BS 8110-85 et européenne CEB-FIP 1990. Des calculs de résistance au poinçonnement ont également été faits à l'aide du logiciel "Response 2000", en utilisant un modèle de poutre équivalente pour la dalle.

Les conclusions de l'étude indiquent que les formules suggérées pour la résistance au poinçonnement des dalles dans les normes canadienne et américaine peuvent être non sécuritaires dans certaines conditions, en particulier pour les dalles épaisses. L'auteur recommande de modifier ces formules afin de tenir compte de cet effet d'échelle.

Acknowledgements

The author wishes to sincerely thank Professor Denis Mitchell for his guidance and encouragement throughout the course of this research program. The patience and invaluable assistance of both Dr. William D. Cook and Stuart Bristowe was also tremendously appreciated.

The research presented in this thesis was carried out in the Jamieson Structures Laboratory at McGill University. The author would like extend special thanks to Ron Sheppard, Marek Przykorski, John Bartzak, and Damon Kiperchuk for their assistance in the laboratory. Special thanks are extended to Dean Dugas for his help in the construction and testing of all the specimens. The author would also like to thank Bryce Tupper, Emmet Poon, Carla Ghannoum, Wassim Ghannoum, Pedro Da Silva and Jamie Paterson for their assistance during this study.

The completion of this project would not have been possible without the patience and valuable help of the secretaries of the Civil Engineering Department, particular Sandy Shewchuk-Boyd, Ann Bless and Anna Dinolfo.

The author would also like to express his deepest gratitude to his parents and his brother for their constant support, patience and understanding. Finally the author would like to thank his friends David Fung, Charles Mui and Tomas Hoi, for their encouragement's and support throughout his stay at McGill University.

Kevin Ka Lun, Li
March, 2000

Table of Contents

Abstract	i
Résumé	ii
Acknowledgements	iii
Table of Contents	iv
List of Figures	vi
List of Tables	viii
List of Symbols	ix
1 Introduction and Literature Review	1
1.1 Introduction	1
1.2 Previous Research on Punching Shear Resistance of Two-Way Slabs	2
1.3 Current Code Provisions for Punching Shear Strength of Two-Way Slabs	8
1.4 Previous Research on Size Effect Investigations	10
1.5 Current Code Provisions for Shear Strength of One-Way Slabs and Beams Without Transverse Reinforcement	12
1.6 Research Objectives	13
2 Experimental Programme	14
2.1 Design and Details of the Slab Specimens	14
2.2 Material Properties	19
2.2.1 Reinforcing Steel Properties	19
2.2.2 Concrete Properties	21
2.3 Testing Procedure.....	24
2.3.1 Test Setup and Loading Apparatus	24
2.3.2 Instrumentation.....	25
3 Response of Two-Way Slab Specimens	26
3.1 Specimen P100.....	26
3.2 Specimen P150.....	29
3.3 Specimen P200.....	32
3.4 Specimen P300.....	35
3.5 Specimen P400.....	38
3.6 Specimen P500.....	41
3.7 Summary of Results	44

4 Analysis of Test Results	46
4.1 Comparison of Two-Way Slab Test Results	46
4.1.1 Load-Deflection Responses.....	46
4.1.2 Strain Distribution of Reinforcing Steel.....	49
4.2 Comparison of Predictions with Failure Loads	51
4.3 Predictions Using the Modified Compression Field Theory	57
5 Conclusions	60
5.1 Conclusions of this Experimental Program.....	60
References	62
Appendix A-Response 2000^o Input and Output	66

List of Figures

Chapter 1

- 1.1 Influence of member depth and aggregate size on shear stress at failure for tests carried out by Shioya 1989 11

Chapter 2

- 2.1 Details of test specimen and test setup..... 15
- 2.2 Slab-column test specimen 17
- 2.3 Typical distribution of flexural tension reinforcement 17
- 2.4 Slab reinforcement details 18
- 2.5 Typical tensile stress-strain curves for reinforcing steel 20
- 2.6 Typical compressive stress-strain curves for concrete 22
- 2.7 Concretes shrinkage strains 23
- 2.8 Photographs of test setup for two-way slab specimens..... 24
- 2.9 Strain gauge locations on top mat reinforcement..... 25

Chapter 3

- 3.1 Load versus average deflection responses of Specimen P100 27
- 3.2 Failure at slab-column connection for Specimen P100 27
- 3.3 Strains in tension reinforcing bars at full service and peak load for Specimen P100..... 28
- 3.4 Load versus average deflection responses of Specimen P150 30
- 3.5 Failure at slab-column connection for Specimen P150 30
- 3.6 Strains in tension reinforcing bars at full service and peak load for Specimen P150..... 31
- 3.7 Load versus average deflection responses of Specimen P200 33
- 3.8 Failure at slab-column connection for Specimen P200 33
- 3.9 Strains in tension reinforcing bars at full service and peak load for Specimen P200..... 34
- 3.10 Load versus average deflection responses of Specimen P300 36
- 3.11 Failure at slab-column connection for Specimen P300 36
- 3.12 Strains in tension reinforcing bars at full service and peak load for Specimen P300..... 37
- 3.13 Load versus average deflection responses of Specimen P400 39
- 3.14 Failure at slab-column connection for Specimen P400 39
- 3.15 Strains in tension reinforcing bars at full service and peak load for Specimen P400..... 40
- 3.16 Load versus average deflection responses of Specimen P500 42
- 3.17 Failure at slab-column connection for Specimen P500 42
- 3.18 Strains in tension reinforcing bars at full service and peak load for Specimen P500..... 43
- 3.19 Shear stress at failure versus specimen depth 45

Chapter 4

4.1	Comparison of load versus average deflection responses of the outer LVDTs for the six slab specimens	48
4.2	Comparison of load versus average deflection responses of the inner LVDTs for the six slab specimens	48
4.3	Comparison of experimental and predicted failure loads.....	52
4.4	Comparison of experimental and predicted failure stress	53
4.5	Comparison of size reduction factors according to different codes.....	54
4.6	Comparison of experimental results and CSA Standard modified with size reduction factor of one way shear	54
4.7	Comparison of experimental results and predicted failure loads by various investigators.....	55
4.8	Response 2000 ^c predictions for distance d from the column face.....	58
4.9	Response 2000 ^c predictions for distance $d/2$ from the column face	59

List of Tables

Chapter 1	
1.1	Comparison of code provisions for nominal shear strength of square column 11
1.2	Comparison of code provisions for nominal shear strength of one-way members 13
Chapter 2	
2.1	The dimensions and steel reinforcement details of the specimens 16
2.2	Reinforcing steel properties 19
2.3	Concrete mix designs 21
2.4	Concrete properties for both series 22
Chapter 3	
3.1	Summary of results 44
Chapter 4	
4.1	Summary of key loads and deflections for slab test specimens 47
4.2	Strain distributions in the strong and weak directions at full service load 49
4.3	Strain distributions in the strong and weak directions at peak load 50
4.4	Comparison of failure loads to code predictions for slab specimens 51
4.5	Comparison of failure loads to predictions using equations proposed by various investigators 55
4.6	Modified compression field theory predictions by Response 2000 [®] 58

List of Symbols

a	shear span
A_c	area of concrete
A_s	area of longitudinal steel reinforcement
b	perimeter of loaded area
b_o	perimeter of critical section for shear
b_w	minimum effective web width within depth d
c	size of rectangular or equivalent rectangular column
d	effective depth of slab
d_b	nominal diameter of reinforcing bars
f'_c	specified compressive strength of concrete
f_{cu}	limiting compressive stress in concrete strut
f_r	modulus of rupture of concrete
f_{sp}	splitting tensile stress of concrete
f_u	ultimate strength of reinforcement
f_y	yield strength of reinforcement
h	overall thickness of specimens
L	overall width of specimens
n	ratio of tension steel through loaded area to total area of tension steel in slab
s	spacing of tension reinforcement
v	nominal shear strength
v_c	shear stress resistance provided by concrete
V	shear force at failure
V_c	shear force resistance attributed to the concrete
α_1	ratio of average stress in rectangular compression block to the specified concrete strength
β	tensile stress factor which accounts for the shear resistance of cracked concrete
ϵ'_c	concrete strain at f'_c
ϵ_s	tensile strain in tensile tie reinforcement
ϵ_y	yield strain of reinforcement
ϵ_{sh}	ultimate strain of reinforcement
ϕ_c	resistance factor for concrete
ϕ_s	resistance factor for reinforcement
ϕ_o	ratio of ultimate load to the load at which flexural failure should occur
γ_c	partial safety factor
λ	factor to account for concrete density
ρ	ratio of longitudinal tension reinforcement, A_s/bd
ξ	$1+(200/d)^{1/2}$ (size effect term)

Chapter 1

Introduction and Literature Review

1.1 Introduction

Punching shear failures of concrete flat plate structures are undesirable modes of failure since they give little warning and have catastrophic consequences. Therefore, it has been of special interest to engineers to try to understand the behaviour of slab-column connections. However, although extensive research has been done on the punching shear strength of slabs, to date there is still no generally applicable, rational theory. The current building code design procedures are based on empirical studies and concerns have been raised about their ability to accurately predict the punching shear strength of slabs for all situations. This lack of understanding is more evident in the shear design provisions of the ACI Code (ACI committee 318-1995) which consists of 43 empirical equations for different types of members and different loading conditions. Moreover, there is great discrepancy between design codes of different countries. Many of these codes do not even account for some basic and proven factors affecting the shear capacity of concrete members. Of these factors, much confusion is expressed with regards to the effect of member size on the shear capacity of slab elements. The focus of this research is to investigate the “size effect” in normal-strength concrete slabs in order to better understand the mechanisms involved.

This chapter will give a brief overview of the previous research on punching resistance of two-way slabs and size effect investigations. The current punching shear strength provisions used in the various codes will also be discussed.

1.2 Previous Research on Punching Shear Resistance of Two-Way Slabs

In the early 1900's, E. Mörsh of Germany made significant contributions to the understanding of the behavior of reinforced concrete structures with his work on shear. In his 1906 and 1907 papers, Mörsh presented an explanation of diagonal tension and proposed the following expression for the nominal shearing stress, v :

$$v = \frac{V}{bd} \quad (1.1)$$

where V is the applied shear force,

b is the perimeter of the loaded area, and,

d is the effective depth.

The shear stress from Mörsh's equation is calculated along the perimeter, b , of the loaded area. Hence, for a uniformly loaded slab, the shear stress was evaluated around the perimeter of the column.

Talbot (1913) published a report of 114 wall footings and 83 column footings tested to failure. Twenty of these footings failed in shear. They exhibited failure surfaces that were at an angle of approximately 45° to the vertical and that extended from the bottom face of the slab at its intersection with the column, reaching the level of the reinforcement at a distance d from the column face. From these test findings, Talbot concluded that it would be reasonable to take the vertical section located at a distance d from the face of the column as the critical shear section. He proposed the following expression for the nominal shearing stress, v , which is similar to Mörsh's, except that the critical section was moved from the face of the column to a distance d from the face. Therefore b was now equal to $4(c+2d)$, giving:

$$v = \frac{V}{4(c+2d)d} \quad (1.2)$$

where c is the length of one face of a square column.

Talbot also recognized that increased percentages of flexural reinforcement resulted in an increase in the shear strength of the slabs.

In 1924, the ACI code committee reported that the diagonal shear stress appeared to be critical at a distance ($h-1.5$ in.) from the periphery of the loaded area, where h is the slab thickness. Furthermore, the committee recommended that the shear stress, which is a working stress limit, be limited to:

$$v = 0.02f'_c (1 + n) \leq 0.03f'_c \quad (1.3)$$

where f'_c is the concrete compressive strength in MPa, and,

n is the area of steel in the loaded region divided by the total area of steel in the slab.

Graf (1933) studied the shear strength of slabs loaded by concentrated loads near the supports. From the test findings, he concluded that the shear capacity decreases as the loads move away from the supports and that flexural cracking had some influence on shear strength. Graf also proposed the following expression for the shear stress:

$$v = \frac{V}{4ch} \quad (1.4)$$

where h is the thickness of the slab..

Richart (1948) presented a report on a number of reinforced concrete footing tests. He concluded that the high tensile stresses in the flexural reinforcement lead to extensive cracking in the footings. This cracking reduced the shear strength, resulting in the footings failing at lower shearing stresses than expected.

Elstner and Hognestad (1956) reported on tests of thirty-four 6 feet square slabs that exhibited punching shear modes of failure. In two of these slabs, 50% of the flexural reinforcement was concentrated over the column. They then compared these two slabs with two others that were similar except that the flexural reinforcement was uniformly distributed throughout the width of the slabs. They concluded that concentrating the flexural reinforcement near the column did not result in any increase in the punching shear strength of the slab specimens. Elstner and Hognestad (1956) also revised an

earlier formula initially proposed by Hognestad in 1953, to evaluate the ultimate shear strength of slabs. The revised expression is as follows:

$$v = \frac{V}{\frac{7}{8}bd} = 2.3 + 0.046 \frac{f'_c}{\phi_o} \quad (\text{N and mm}) \quad (1.5)$$

where ϕ_o is the ratio of the ultimate load to the load at which flexural failure should occur, and b is the perimeter of the loaded area.

Whitney (1957) reviewed the results of slab tests by Richart (1948), Elstner and Hognestad (1956). He reported that in these tests the slab specimens that had a high percentage of reinforcement probably also failed due to bond failure and not shear. Furthermore, Whitney proposed an ultimate shear strength theory and concluded that the shear strength is primarily a function of the “pyramid of rupture”, which is a pyramid with surfaces sloping out from the column at angles of 45° .

The 1956 ACI Building Code recommended two different limits for shear stresses in slabs at a distance d away from the periphery of the loaded area:

$$v \leq 0.03 f'_c \leq 0.69 \text{ MPa,}$$

if more than 50% of the flexural reinforcement passes through the periphery; or

$$v \leq 0.025 f'_c \leq 0.59 \text{ MPa,}$$

if only 25% of the flexural reinforcement passes through the periphery.

Kinnunen and Nylander (1960) proposed a rational model for predicting punching shear behaviour in slabs. Basically, in this model the slab is divided into rigid radial segments, each bounded by two radial crack lines, the periphery of the column or loaded area where the initial circumferential crack usually forms the slab boundary. Before failure occurs, the main deformation of each radial segment is a rotation around a centre of rotation (C.R.) located at the periphery of the column and at the level of the neutral axis. Failure takes place when the frontal part of the radial segment fails to support the force at the column face, that is the concrete crushes in the tangential direction.

Moe (1961) tested forty-three 6 feet square slab specimens and reviewed the test findings from 260 slabs and footings tested by previous investigators. He concluded that the shear strength of slabs is to some extent dependent upon the flexural strength. He also

concluded that the concentration of the flexural reinforcement does not result in an increase in the shear strength, but does increase the stiffness of the load-deformation response and increase the load at which initial yielding occurs. He proposed the following expression for evaluating the ultimate shear strength of slabs:

$$v_u = \frac{V_u}{bd} = \left[15 \left(1 - 0.075 \frac{c}{d} \right) - 5.25 \phi_s \right] \sqrt{f'_c} \quad (\text{N and mm}) \quad (1.6)$$

Regan (1974) reviewed previous research by various investigators on the punching shear strength of slabs. He noted that the shear strength increases with increasing reinforcement ratios and concrete strengths, but the effect is less than linear. Hence, the rate of increase of shear strength should decrease at higher reinforcement ratios and concrete strengths.

Hawkins and Mitchell (1979) reported that in a punching shear failure the shear strength is dependent on the flexural capacity of the slab and that it will decrease if there has been significant yielding of the flexural reinforcement.

Rankin and Long (1987) proposed a method for determining the punching shear strength of conventional slab-column connections based on rational concepts of the modes of failure of these connections. They proposed the following punching shear strength expression:

$$P_{vs} = 1.66 \sqrt{f'_c} (c+d) \times d \times \sqrt[4]{100\rho} \quad (\text{N and mm}) \quad (1.7)$$

where f'_c is the compressive strength in MPa,

ρ is the reinforcement ratio, A_s/bd , and,

P_{vs} is the punching shear strength.

Alexander and Simmonds (1988) noted that the CSA Standard (1984) ensures that a large portion of the flexural reinforcement pass through or near the column. However, they recognized that there was little indication as to how the amount of reinforcement actually affects the punching shear strength. They believed that there should be a

beneficial effect for the amount of flexural reinforcement to be included in the calculations for the shear strength capacity in the CSA Standard.

Shehata and Regan (1989) proposed a mechanical model to estimate the punching resistance of slabs. The model was based on test observations as well as numerical analyses. The authors believed that their model was an improvement over that of Kinnunen and Nylander (1960) as it included the influence of the deformation of the part of the slab on the top of the column and bounded by the shear crack. Furthermore, they suggest that their model provides a more complete definition of failure. Shehata and Regan also performed a parametric study of their theoretical model and of the American Code and the British Standard approaches. This study revealed that the British Standard results were closer to their theory in accounting for the steel ratio, which the ACI Code ignores.

Alexander and Simmonds (1992) studied the effects of concentrating the reinforcement near the column on the shear strength of slab specimens. They concluded that all the tests exhibited the classical pyramid shaped punching shear failure, but several tests actually had loss of anchorage. The anchorage failures were not distinguishable from punching shear failures on the basis of external appearances. They suggested that many of the punching shear failures reported in the previous tests were actually bond failures. They believed that investigators such as Moe, Elstner and Hognestad wrongly diagnosed the mode of failure in many of their tests and that it prevented them from observing an improvement in the shear capacity of slabs with the concentration of the flexural reinforcement near the column.

Gardner and Shao (1996) reported the experimental results for the punching shear of a two-bay by two-bay reinforced concrete structure. They reviewed the code provisions of the ACI 318-89 Code, the BS 8110-85 Standard, and the CEB-FIP 1990 Model Code, and compared these predicted values to previous experimental research from various investigators. They concluded that the code equations that included size effects and reinforcement ratios (such as the BS 8110-85 and CEB-FIP Model Code equations) had smaller coefficients of variation than the ACI expressions. They also noted that a parametric study by Shehata and Regan showed that the punching shear strength is approximately proportional to the cube root of the concrete strength, steel

ratio, and steel yield stress. This led them to derive a shear stress expression that includes these various parameters. The equation is as follows:

$$v_u = \frac{V_u}{b_o d} = 0.79 \times \sqrt{1 + (200 / d)} \times \sqrt[3]{\rho f_y} \times \sqrt[3]{f_{cm}} \times \sqrt{(d / b_o)} \quad (\text{N and mm}) \quad (1.8)$$

where f_{cm} is the mean concrete strength, in MPa, and b_o is the perimeter of the loaded area. Gardner and Shao also cautioned that although increasing the amount of flexural reinforcement increases the punching shear capacity of the slab-column connection, it results in a more brittle behaviour.

Sherif and Dilger (1996) reviewed the CSA A23.3-94 punching shear strength provisions for interior columns. After comparing these provisions to results from previous research experiments, they concluded that these provisions can be unsafe under certain conditions, particularly for slabs with low reinforcement ratios ($\rho < 1\%$). They also noted that since most slab design has a reinforcement ratio, ρ , of less than 1% it is important that the code equations for the shear strength be modified to include ρ . In addition, they also concluded that the shear resistance of slabs decreases with increasing depth. They suggested that these provisions can be unconservative for thick slabs. For slabs with $d > 300$ mm, they recommended the use of size factors used by the Canadian Code for one-way shear, while for slabs with $d \leq 300$ mm, a size factor is not required. They proposed the following design equation for the punching shear resistance at failure:

$$v = 0.7 \sqrt[3]{100 \rho f_c'} \left(\frac{1300}{1000 + d} \right) \quad (\text{N and mm}) \quad (1.9)$$

1.3 Current Code Provisions for Punching Shear Strength of Two-Way Slab

The current understanding of the mechanics involved in the punching shear failures in flat slab structures is based mainly on experimental research programs conducted to investigate the behaviour and strength of conventional slab-column conditions. Due to the differences in the previous research, there exists a significant variation in the methods of evaluation of the punching shear capacity of slabs in the concrete codes of North America, Europe and Britain. The American ACI Code and Canadian CSA Standard are largely based on the work of the German investigator Moe, while the European and British codes are primarily based on Regan's work. The equations used to determine the nominal shear strength in the CSA Standard, the ACI Code, the BS Standard and the CEB-FIP Model Code are compared in Table 1.1. The expression given in Table 1.1 for the ACI Code and the CSA Standard is for a circular column or a rectangular column with an aspect ratio of long to short side of two or less. For aspect ratios greater than 2.0 or for very large lengths of shear periphery, the shear stress at failure is reduced.

Table 1.1 Comparison of code provisions for nominal shear strength for square columns

Code	Critical Periphery, b_o	Nominal Shear Strength
CSA 23.3-94 ACI 318-95	Located at $d/2$ from column face $b_o = 4(c + d)$ for square column	$v = (0.33 \times \sqrt{f'_c})$
S 8110-85	located at $2d$ from column face $b_o = 4(c + 3d)$ for square column	$v = 1.05 \times \sqrt[3]{100\rho} \times \sqrt[4]{400/d}$ multiply by $\sqrt[3]{f'_c/25}$ for $f'_c > 25$ MPa but f'_c is limited to 40 MPa where, ρ = ratio of steel within $1.5d$ of column face. $\sqrt[4]{400/d}$ should not be taken as less than 1
CEB-FIP 1990	located at $2d$ from column face $b_o = 4(c + \pi d)$ for square column	$v = 0.16 \times \xi \times \sqrt[3]{100\rho f'_c}$ where, $\xi = 1 + \sqrt{200/d}$

The ACI 318-95 Code (1995) does not include the amount of flexural reinforcement in its shear strength calculations. The current CSA A23.3-94 Standard (1994) requires that half of the flexural reinforcement needed in the column strip be placed within 1.5 times the slab thickness, h , either side of the column face, but does not give beneficial effects for this distribution in the calculation of the shear strength. Neither the American Code or the Canadian Standard include a size effect term in their expressions for shear strength and both use the relation $v \propto \sqrt{f'_c}$. It is noted that the 1994 CSA Standard uses a factored shear stress at failure of $0.4 \phi_c \sqrt{f'_c}$, where ϕ_c is the material resistance factor for concrete, equal to 0.60. The factor of 0.4 in this expression was increased from 0.33 to 0.4 to account for the low value of ϕ_c . Hence, the nominal shear stress resistance should be taken as $0.33\sqrt{f'_c}$. The CEB-FIP Model Code (1990) and the BS-8110 Standard (1985) include the flexural reinforcement concentration and a size effect term in their calculations of the shear resistance of the connection. They both use the relation $v \propto \sqrt[3]{f'_c}$. In addition the BS Standard limits f'_c to 40 MPa in computing the shear strength and the CEB-FIP Model Code sets its limit on f'_c to 50 MPa. Although the coefficient in the design shear stress equation is 0.12 in the CEB-FIP Model Code, Regan (1999) has indicated that a coefficient of 0.16 (see Table 1.1) represents the nominal shear stress at failure. Although the coefficient for the design expression in the BS Standard is 0.79, using the same partial safety factor of 1.33 suggested by Regan results in an increase in this factor to 1.05 for the nominal resistance (see Table 1.1).

1.4 Previous Research on Size Effect Investigations

There has been little research on the size effect of the punching shear failure of two-way slabs. Most of the investigations on size effect of the shear strength are for beams or one way slabs. Kani (1966 and 1967) was among the first to investigate the effect of member size on concrete shear strength. He tested four series of beams without web reinforcement with varying member depths, d , longitudinal steel percentages, ρ , and shear span-to-depth ratios, a/d . He concluded that member depth and steel percentage had a great effect on shear strength and there is a transition point at $a/d \approx 2.5$ at which beams are shear critical.

It was found that the value of a/d to be the transition point between failure modes and is the same for different member sizes and steel ratios. For an a/d value greater than 2.5, failure was sudden, brittle and in diagonal tension soon after the first cracks appeared. For an a/d value lower than 2.5, the test specimens developed arch action and had a considerable reserve of strength beyond the first cracking point. This transition point is more evident in test specimens with higher reinforcement ratios and almost disappears in test specimens with lower reinforcement ratios.

Bazant and Kim (1984) proposed a shear strength equation based on the theory of fracture mechanics. This equation accounts for the size effect phenomenon and the longitudinal steel ratio was calibrated using 296 previous tests obtained from the literature. They concluded that for very large specimen depths, the safety factor in the ACI Code almost disappears. However, apart from Kani's test, no experimental evidence was available yet to confirm that fact as all the tests performed up to that time were on relatively small specimens.

Sohiya (1989) conducted a number of tests on large-scale beams in which the influence of member depth and aggregate size on shear strength was investigated. Lightly reinforced concrete beams, varied in depth from 100 mm to 3000 mm, containing no transverse reinforcement were tested under a uniformly distributed load. Sohiya concluded that the shear stress at failure decreased as the member size increased and as the aggregate size decreased. Figure 1.1 illustrates the results obtained by Shioya.

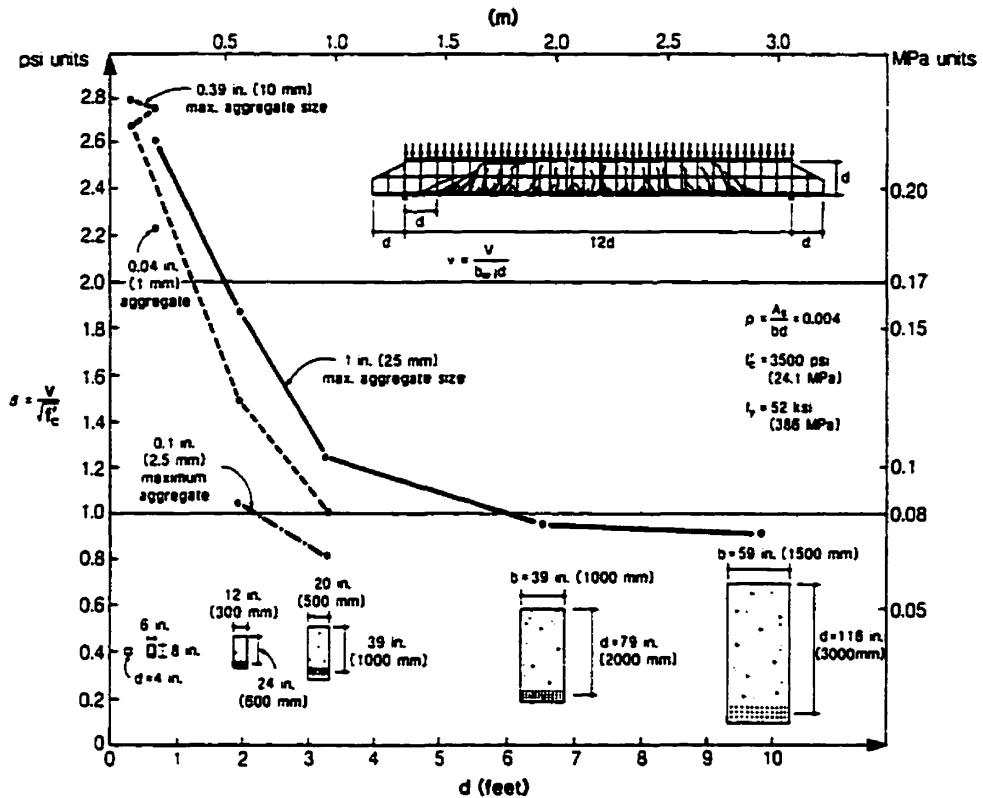


Figure 1.1 Influence of member depth and aggregate size on shear stress at failure for tests carried out by Shioya 1989 (Source: Collins and Mitchell, 1997)

Bazant and Kazemi (1991) reported on tests on geometrically similar beams with a size range of 1:16 and having a constant a/d ratio of 3.0 and a constant longitudinal steel ratio, ρ . The depth of specimens varied from 1 inch (25mm) to 16 inches (406mm). The main failure mode of the tested specimens was diagonal shear but the smallest specimen failed in flexure. This study confirmed the size effect phenomenon and helped corroborate the previous published formula. Since the deepest beams tested was relatively small, Bazant and Kazemi concluded that for beams larger than 16 inches (406mm) additional reductions in shear strength due to size effect were likely.

Collins and Mitchell (1991) introduced a design approach for shear, based on the modified compression field theory (Vecchio and Collins 1986, Collins et al. 1996). The design approach was adopted by the 1994 CSA Standard and the AASHTO LRFD specifications (AASHTO, 1994). For members without transverse reinforcement, this design approach includes a size effect by relating the crack spacing to the effective depth.

d of the member. Members, without stirrups, therefore have larger crack spacing as they get deeper and consequently the model predicts larger crack widths and hence smaller crack-slip resistance. Collins and Mitchell (1991) demonstrated the accuracy by predictions using this approach on the size-effect series tested by Shioya (1989). Additional tests on size effect are reported by Collins et al. (1993) which clearly showed the importance of size effect in beams without transverse reinforcement.

1.5 Current Code Provisions for Shear Strength of One-Way Slabs and Beams Without Transverse Reinforcement

The ACI Code (1995) shear design equations for non-prestressed reinforced concrete beams were derived in 1962 based on tests involving relatively small ($d_{avg} = 340$ mm) and rather heavily reinforced ($\rho_{avg} = 2.2\%$) beams and do not recognize the size effect on the shear performance. The equations for predicting the shear strength of concrete beam elements are based on the shear causing significant diagonal cracking. In addition to the General Method using modified compression field theory, which includes a size effect and also accounts for amount of flexural reinforcement, the CSA Standard (1994) provides a simplified design expression. It includes a term to account for the size effect in its shear design expression but does not take account of the reinforcing steel ratio, ρ . This shows the concern of this code regarding the size effect phenomenon. It is noted that the 1994 CSA Standard uses a factored shear stress at failure of $V_c = 0.2\phi_c\sqrt{f'_c}b_wd$ where ϕ_c is the material resistance factor for concrete, equal to 0.60. The factor of 0.2 in this expression was increased from 0.166 to 0.2 to account for the low value of ϕ_c . Hence, the nominal resistance can be taken as $V_c = 0.166\sqrt{f'_c}b_wd$. The equations used to determine the nominal shear strength in the CSA Standard and the ACI Code are compared in Table 1.2.

Table 1.2 Comparison of code provisions for nominal shear strength of one-way members

Code	Nominal Shear Strength
ACI 318-95	$V_c = 0.166\sqrt{f'_c} b_w d$
CSA 23.3-94	<p>(a) Simplified Method</p> <ul style="list-style-type: none"> For sections having either the minimum amount of transverse reinforcement required in the Standard or an effective depth, d not exceeding 300 mm $V_c = 0.2\phi_c\sqrt{f'_c} b_w d$ <ul style="list-style-type: none"> For sections with effective depths greater than 300 mm with no transverse reinforcement or less transverse reinforcement than the minimum required $V_c = \left(\frac{260}{1000 + d}\right)\phi_c\sqrt{f'_c} b_w d \quad \text{not less than} \quad 0.10\phi_c\sqrt{f'_c} b_w d$ <p>(b) General Method</p> <ul style="list-style-type: none"> Accounts for member size, moment shear interaction and distribution of longitudinal reinforcement

1.6 Research Objectives

The objective of this research program is to investigate the “size effect” in punching shear. An experimental program is planned to investigate the reduction in punching shear stress at failure as the thickness of the slab increases. Six slab column specimens were designed and detailed according to the ACI Standard (1995) and the CSA Standard (1994). All specimens were instrumented to enable their variations behavioural aspects to be studied as each test was carried out. The test results obtained from this experimental program will be compared to the ACI Code, the CSA Standard, the BS Standard and CEB-FIP Model Code predictions for the punching shear strength of two-way slabs.

Chapter 2

Experimental Program

2.1 Design and Details of the Slab Specimens

Six slab specimens with similar geometry and steel reinforcement were constructed and tested in the Jamieson Structures Laboratory in the Department of Civil Engineering at McGill University. The specimens were cast and tested in an inverted position to facilitate construction and test setup. The concrete compressive strength for all of the specimens is 30 MPa, while the columns have a design concrete strength of 80 MPa. The overall thickness, h , of the slabs varied from 135 mm to 550 mm, while their widths varied from 925 mm to 1950 mm. The stub columns are 300 mm square for the slabs with h greater than 450 mm. For the slabs with h smaller than 450mm, the stub columns are 200 mm square. There is a 30 mm clear concrete cover on the column ties. Specimens were numbered according to their effective depth (in mm) as follows: P100, P150, P200, P300, P400 and P500. Details of the test specimens are given in Fig. 2.1 and Table 2.1.

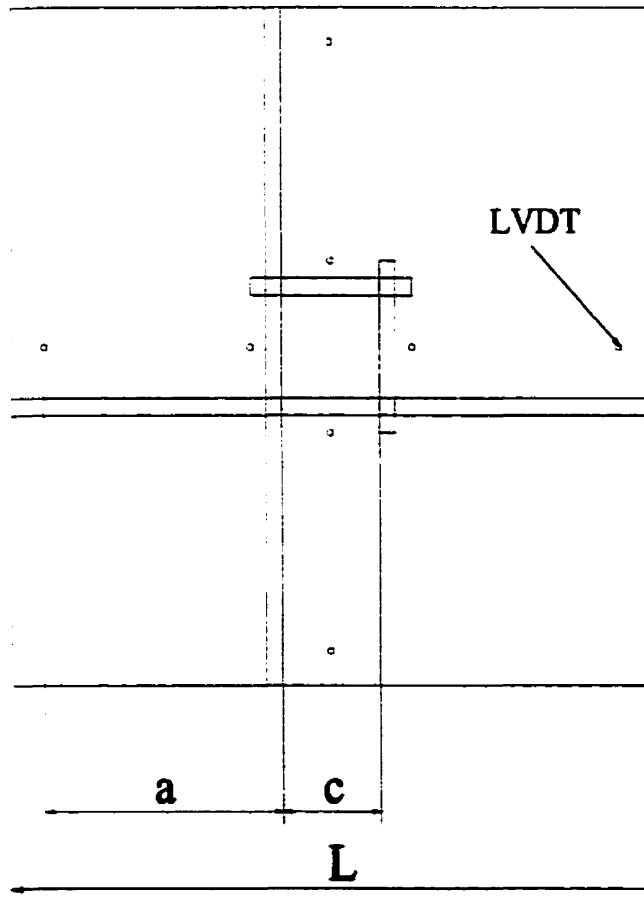
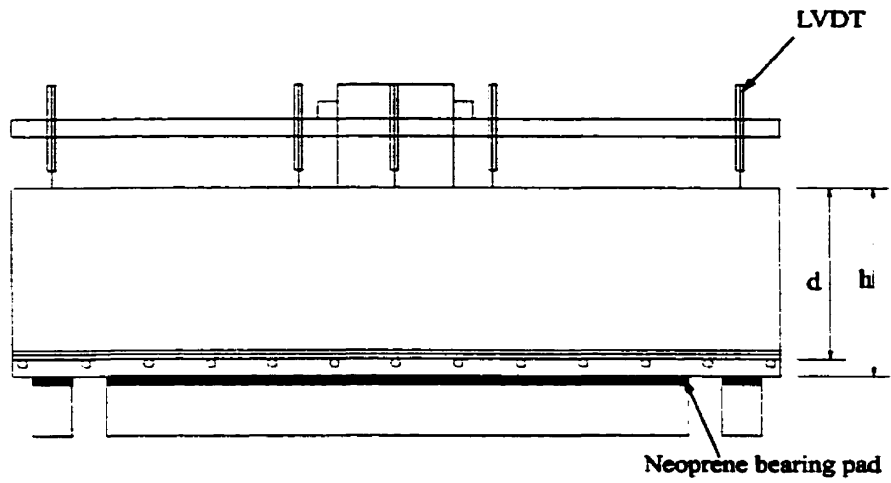


Figure 2.1 Details of test specimen and test setup

Table 2.1 The dimensions and steel reinforcement details of the specimens

Dimensions & Steel Reinforcement	Specimens Designation					
	P100	P150	P200	P300	P400	P500
h (mm)	135	190	240	345	450	550
d* (mm)	100	150	200	300	400	500
c (mm)	200	200	200	200	300	300
L (mm)	925	1190	1450	1975	1975	1975
a (mm)	262.5	395	525	787.5	737.5	737.5
Flexural tension reinforcement	9 No. 10	8 No.15	12 No.15	15 No.20	12 No.25	15 No.25
s (mm)	102.8	48.8	120.8	131.7	164.6	131.7
ρ (%)	0.98	0.90	0.83	0.76	0.76	0.76
Compressive reinforcement (structural integrity)	2 No.10	2 No.10	2 No.15	2 No.20	2 No.20	2 No.25
Column bars	4 No.15	4 No.15	4 No.15	4 No.20	4 No.20	4 No.25
Column hoops	5 No.10	5 No.10	5 No.10	5 No.10	5 No.10	5 No.10

* d is equal to the d_{av} of the top and bottom layer of the tension reinforcement

The reinforcement was distributed uniformly along the width of the specimens, leaving a 25 mm clear concrete cover on both sides. The uniform distribution of reinforcement is representative of a design carried out using the 1995 ACI Building Code. The top reinforcement layouts contained equal number of bars in both the strong and weak directions. Due to the fact that the slab-column specimen was tested upside down, the flexural tension reinforcement was placed near the bottom of the slab. Square steel plates were welded to the ends of every bar to ensure that the reinforcement was properly anchored. The specimen's steel reinforcement details are summarized in Table 2.1 and Fig. 2.2. The flexural tension reinforcement layout is summarized in Fig. 2.3. In order to satisfy the structural integrity requirements of the 1994 CSA Standard, two bars were made continuous through the column in both the strong and weak directions. The column reinforcement consisted of four vertical bars and five No.10 hoops. Figure 2.4 shows the slab reinforcement for the slab column specimens.

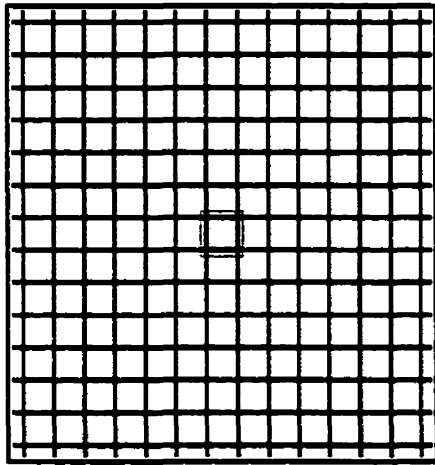


Figure 2.2 Typical distribution of the flexural tension reinforcement

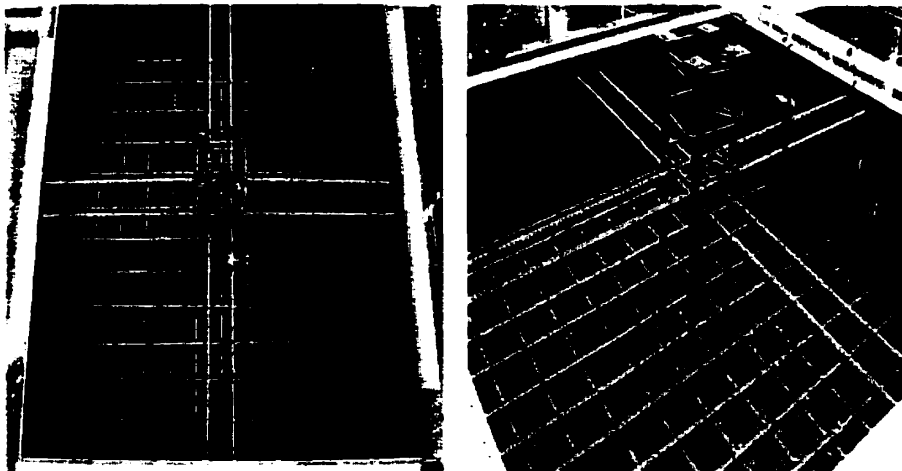


Figure 2.3 Slab reinforcement

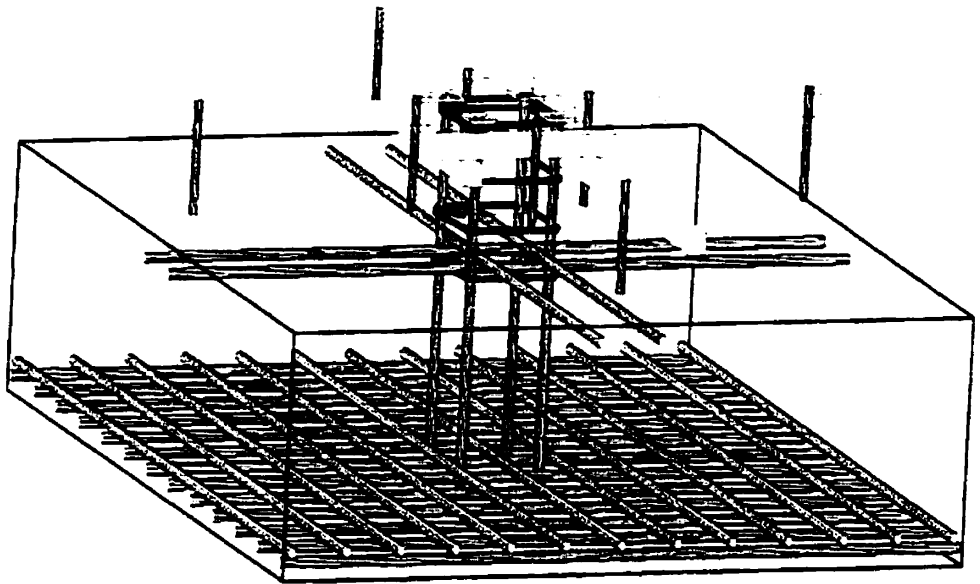
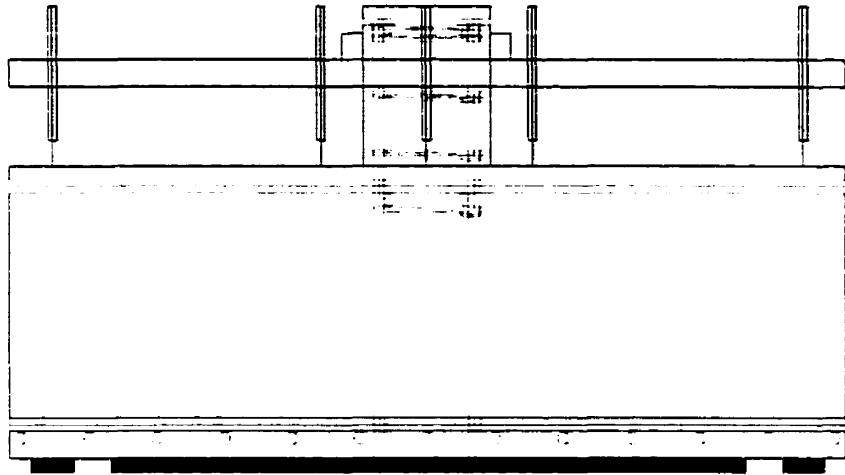


Figure 2.4 Slab reinforcement details

2.2 Material Properties

2.2.1 Reinforcing Steel Properties

The steel reinforcement used in the construction of the specimens consisted of hot-rolled deformed bars with a minimum specified yield stress of 400 MPa. The material properties are summarized in Table 2.2. The values reported are the averages of values obtained from tension tests performed on sample coupons taken from three random bars used. Figure 2.5 shows the typical tensile stress-strain responses of the reinforcing bars, including the yield stress f_y , the ultimate stress, f_u , the yield stress ϵ_y , and the strain at commencement of strain hardening, ϵ_{sh} .

Table 2.2 Reinforcing steel properties

Size Designation	Area (mm ²)	f_y (MPa)	f_u (MPa)	ϵ_y (%)	ϵ_{sh} (%)
No.10 (std. Deviation)	100	488 (6.6)	597 (2.7)	0.24	0.43
No.15 (std. Deviation)	200	465 (3.5)	588 (5.0)	0.23	0.50
No.20 (std. Deviation)	300	468 (1.3)	618 (0.9)	0.23	0.94
No.25 (std. Deviation)	500	433 (1.9)	592 (0.3)	0.22	0.74

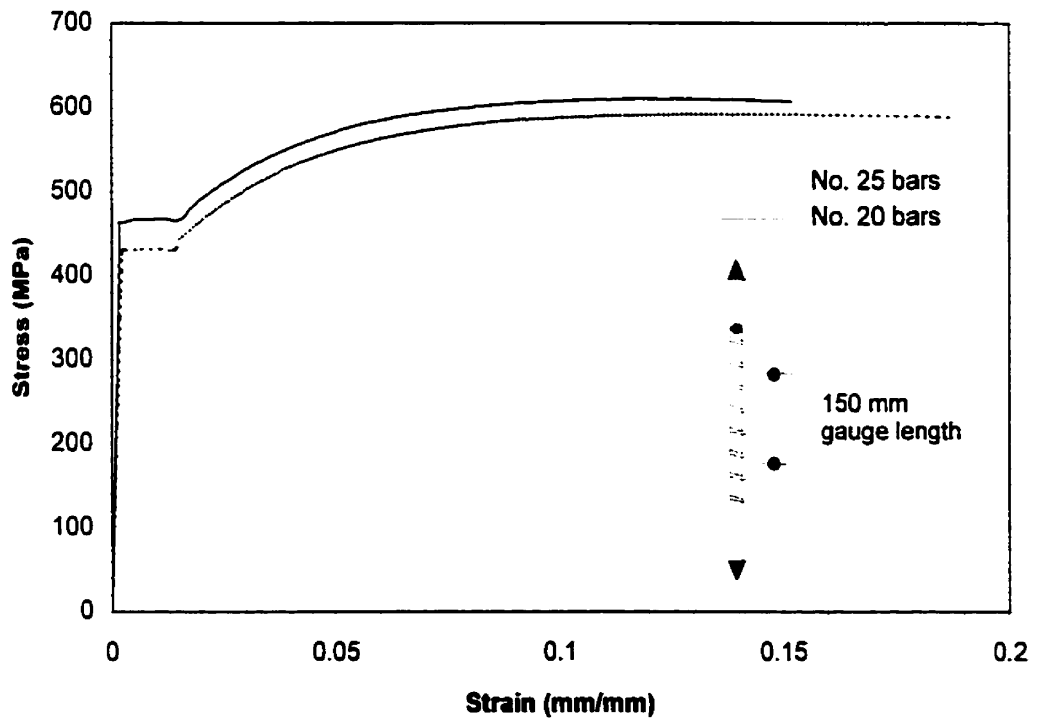
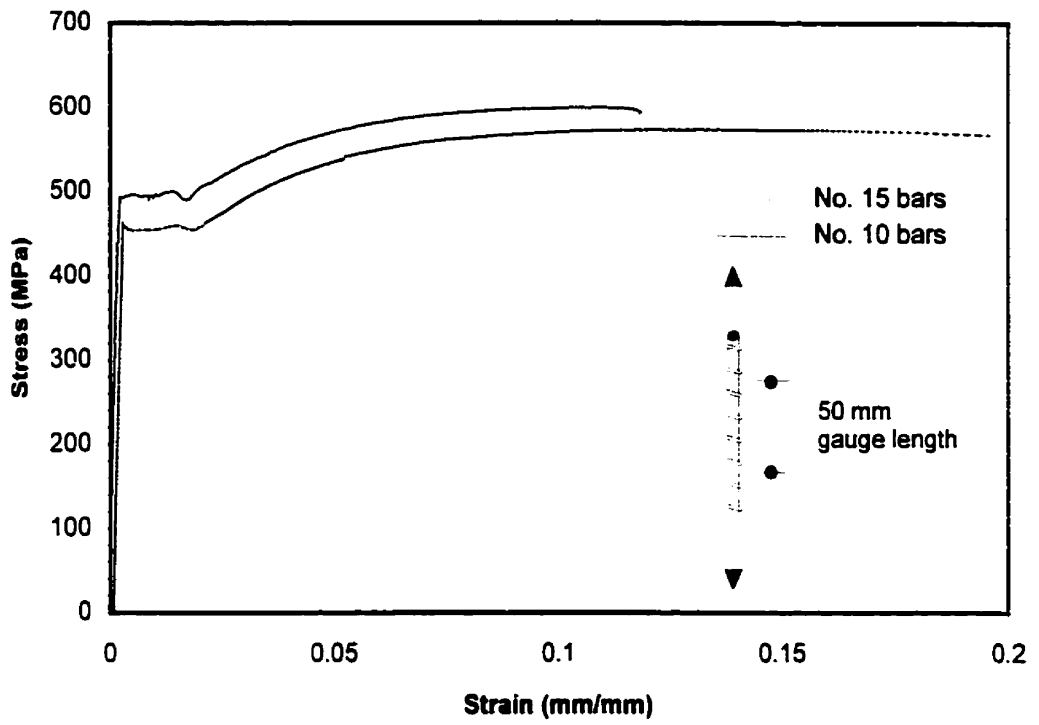


Figure 2.5 Typical tensile stress-strain curves for the reinforcing steel

2.2.2 Concrete Properties

The mix designs for the two different strengths of concrete used to construct the specimens are summarized in Table 2.3. Following the cast, the normal-strength concrete was moist cured for three days and the high-strength concrete was cured for seven days.

Standard cylinders, 150 mm in diameter and 300 mm long, were used for the compression and split-cylinder tests to determine the compressive strength, f'_c , its associated strain ϵ'_c and the splitting tensile stress, f_{sp} . The modulus of rupture, f_r , was determined from 100 mm by 100 mm by 400 mm long flexural beams with three point loading. At least three tests were conducted in order to obtain the mean values of these material properties. The test results are summarized in Table 2.4. Figure 2.6 shows the typical compressive stress-strain responses for both concrete strengths.

Table 2.3 Concrete mix designs

Characteristics	30 MPa Normal-Strength Concrete	70 MPa High-Strength Concrete
Cement (Type 10), kg/m ³	355	480
Fine aggregates (sand), kg/m ³	790	803
Coarse aggregates, kg/m ³ (max. size, mm)	1040 (20)	1059 (10)
Total water*, kg/m ³	178	135
Water-cement ratio	0.50	0.28
Water-reducing agent, ml/m ³	1110	1502
Superplasticizer, L/m ³	-	13
Air-entraining agent, ml/m ³	180	-
Slump, mm	170	180
air content, %	8.8	-
Density, kg/m ³	2130	2491

* Includes the water in admixtures

Table 2.4 Concrete properties for both series

Series	f'_c (MPa)	ϵ'_c $\times 10^{-3}$	f_{sp} (MPa)	f_r (MPa)
Normal-Strength Concrete (Std. deviation)	39.4 (0.31)	2.13 (0.16)	3.27 (0.17)	3.26 (0.24)
High-Strength Concrete (Std. deviation)	79.8 (0.57)	2.97 (0.31)	4.18 (0.11)	7.09 (0.67)

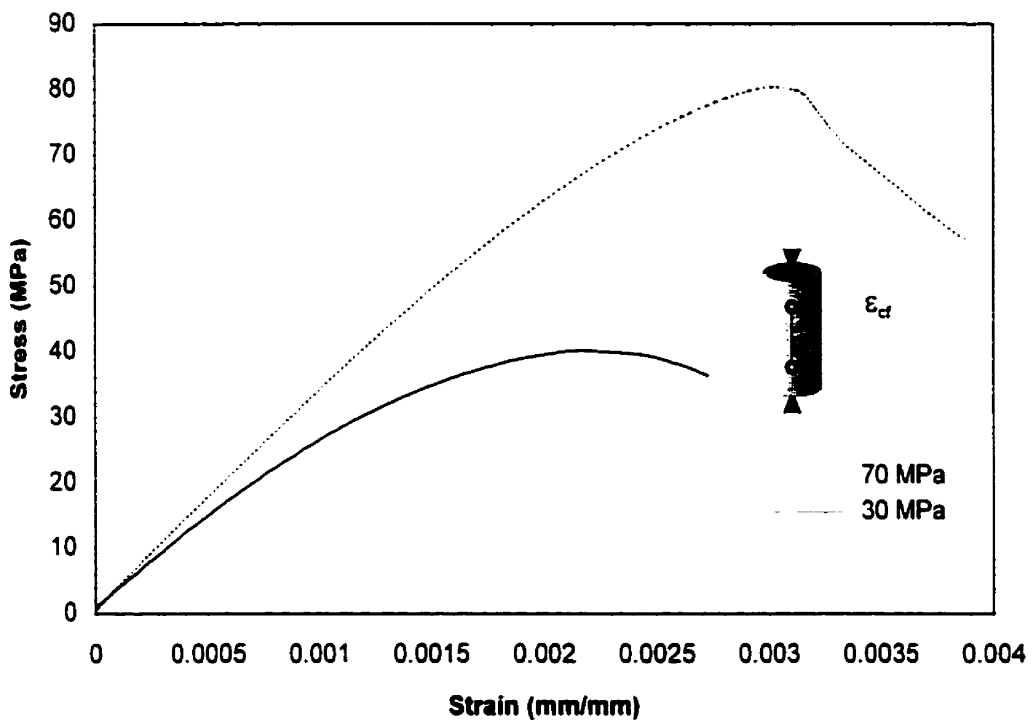


Figure 2.6 Typical compressive stress-strain curves for concrete

Shrinkage measurements were also taken on two standard 50 mm by 50 mm by 275 mm long shrinkage specimens which were cast and cured in the same environment as the full scale specimens. The readings were taken between two small studs embedded in either end of the concrete prisms. The variations of shrinkage versus time are shown in Fig. 2.7.

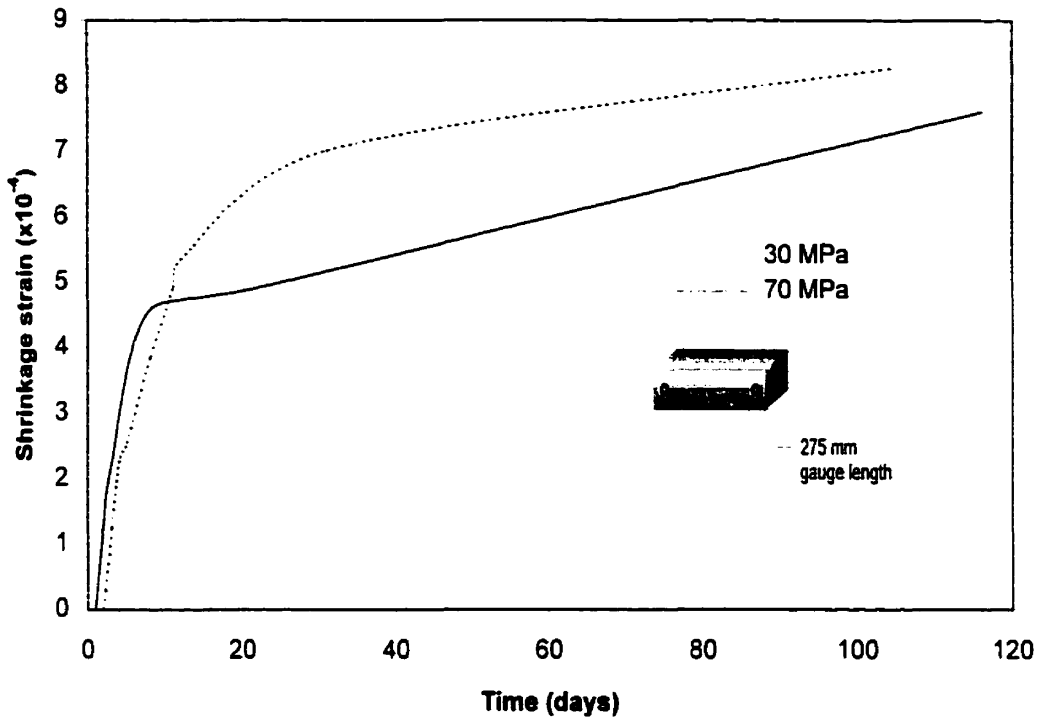


Figure 2.7 Concrete shrinkage strains

2.3 Testing Procedure

2.3.1 Test Setup and Loading Apparatus

All specimens were tested under the MTS universal testing machine in the Jamieson Structures Laboratory of the Department of Civil Engineering at McGill University. The specimens were tested in an inverted position in order to facilitate the test up. The specimens were supported on four lengths of hollow structural sections (HSS); each centered at 100 mm from the outside edge. The head of the MTS machine was seated in capping compound on the top of the column of each specimen. The load was applied monotonically, with the load, deflection and strain values being recorded at each load increment. At key load stages, the crack pattern was recorded. Figure 2.8 shows the test setup for the two-way slab specimens.



Figure 2.8 Photographs of test setup for two-way slab specimens

2.3.2 Instrumentation

Each test specimen was carefully instrumented to provide detailed data on its behaviour throughout its entire loading history. The column load applied to each specimen was obtained from the load cell in the MTS machine. The vertical deflections were monitored with linear voltage differential transformers (LVDTs). A total of eight LVDTs, as shown in Fig. 2.1, were attached to an aluminium section to measure the deflection of the slab relative to the column. Four LVDTs were placed a distance of 100 mm from the outside edge at the centre of each column face. The outer four LVDT's measured the displacement of the slabs at the location of the neoprene bearings, relative to the column. These LVDTs readings were used to detect the start of a punching shear failure. Electrical resistance gauges with a nominal resistance of 120 ohms and a gauge length of 5 mm were glued to the reinforcing bars in the top mat in line with the column face in the two principal directions of the slab as shown in Fig. 2.9. In order to minimize the impact of the gauges on the bond characteristics of the steel, the grinding of the deformations on the reinforcement was kept to a minimum and the protection was confined to the immediate vicinity of the gauges. The steel strain measurements enabled the detection of first yield for each bar passing through the column and the spread of yielding across the width of the test specimen. All the load, displacement and strain readings were recorded with a computerized data acquisition system as each test proceeded.

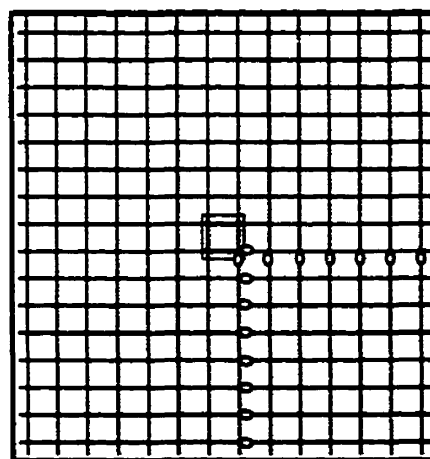


Figure 2.9 Strain gauge locations on top mat reinforcement

Chapter 3

Response of Two-Way Slab Specimens

In this chapter, the observed behaviour of the six slab specimens is presented. Loads, deflections and strains were recorded in order to provide key response data at each load increment. Important load stages included first cracking, full service load, first yielding and failure. The full service is taken as 60% of the nominal shear strength predicted by both the ACI Code and CSA Standard. All of the deflections reported in this chapter are the average of the measured deflections from the four LVDTs, either at the inner location 100 mm from the face of the column or at the outer location over the supports.

3.1 Specimen P100

The total load versus deflection response of Specimen P100, with a concrete strength of 39.4 MPa and a uniform distribution of the top mat of reinforcement, is shown in Fig. 3.1. As can be seen from this figure, the load-deflection curve exhibits a change in stiffness when first cracking occurs at a load of 61 kN. No yielding occurred in the reinforcing bars in both directions. The maximum load was 330 kN with a corresponding average outer deflection of 2.64 mm, before failing abruptly in punching shear. The failure was instantaneous, with the load dropping to 96 kN and the deflection increasing to 11.70 mm. A photograph of Specimen P100 at failure is shown in Fig. 3.2.

Figures 3.3a & 3.3b show the measured strains in the strain gauges in the mat of tension reinforcement at full service load and at the peak load. The highest strains were recorded in the strong direction in the first reinforcing bar, 107 mm away from the centre of the slab, and in the weak direction in the first reinforcing bar, 107 mm away from the

center of the slab. As can be seen from Figure 3.3a, the first reinforcing bar in the strong direction reached 2033 micro-strain at the peak load, while the first bar in the weak direction reached 1802 micro-strain at the peak load as shown in Fig. 3.3b. All measured strains were below the yield strain of the bars (2240 micro-strain).

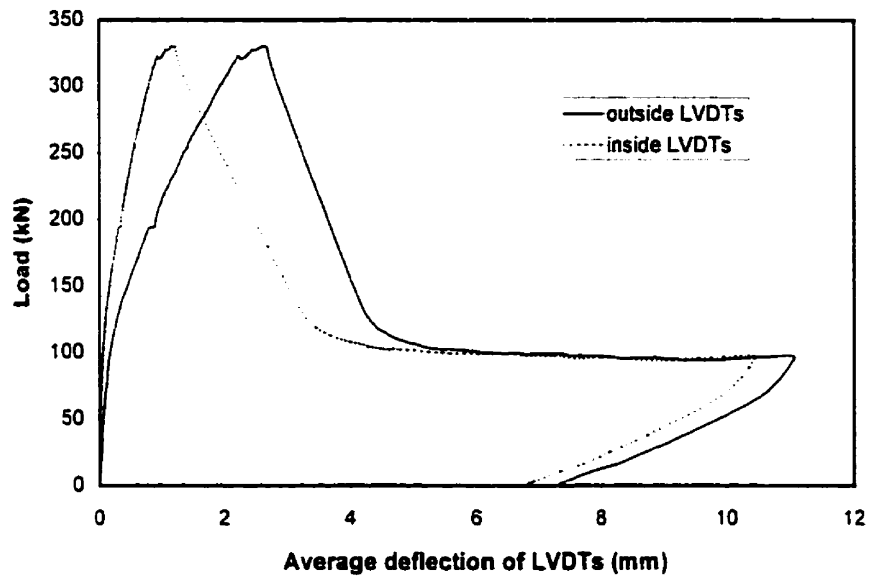


Figure 3.1 Load versus average deflection responses of Specimen P100

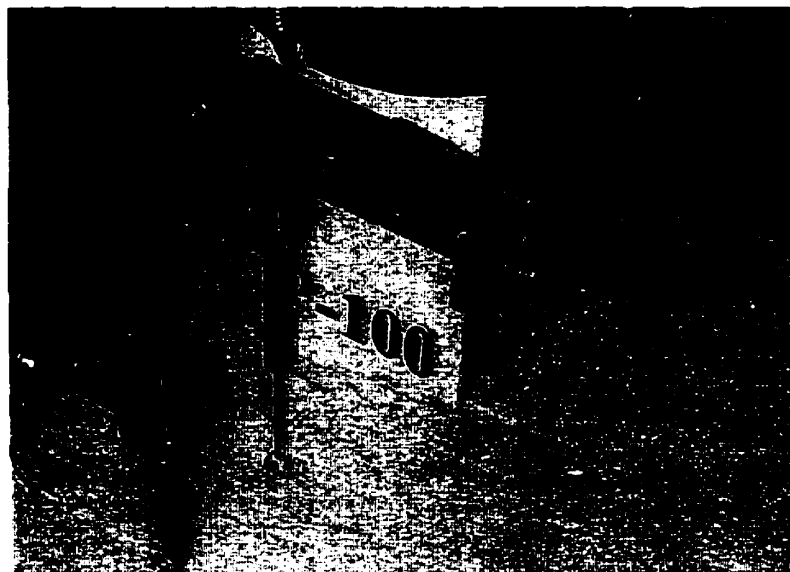
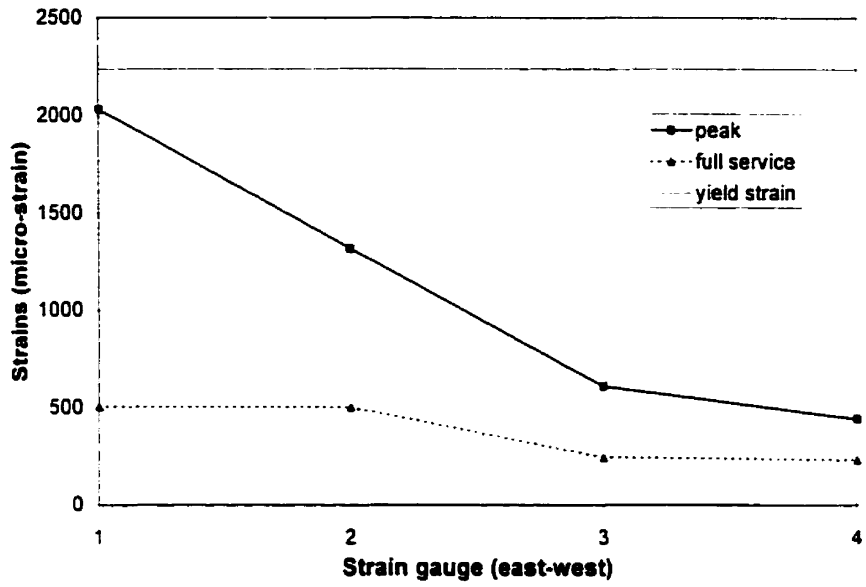
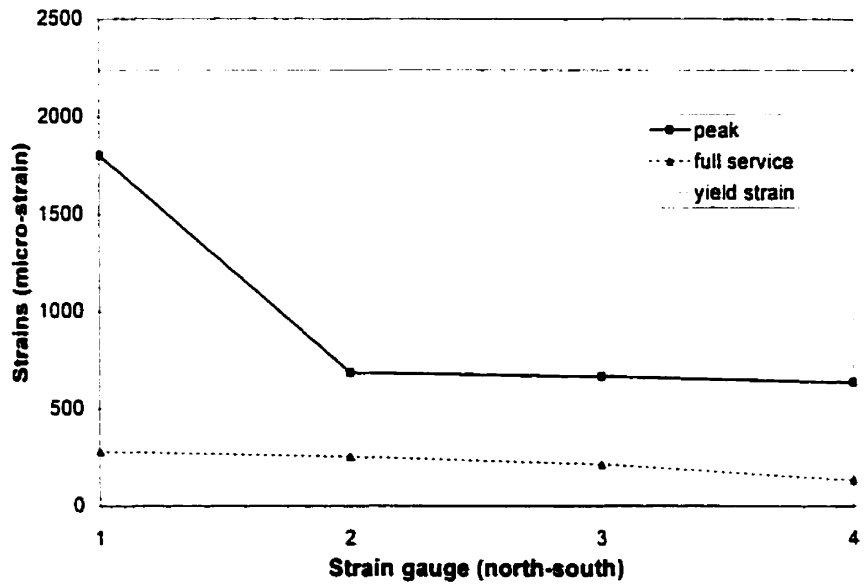


Figure 3.3 Failure at slab-column connection for Specimen P100



a) Strong direction



b) Weak direction

Figure 3.3 Strains in tension reinforcing bars at full service and peak load for Specimen PI00

3.2 Specimen P150

The total load versus deflection response of Specimen P150, with a concrete strength of 39.4 MPa and a uniform distribution of the tension reinforcement is shown in Fig. 3.4. Compared to Specimen P100, the load-deflection curve was stiffer up to the point of first cracking at a load of 154 kN. The maximum load reached was 583 kN with a corresponding deflection of 3.75 mm, before failing abruptly in punching shear. No yielding occurred in the reinforcing bars. The failure was instantaneous, with the load dropping to 173 kN and deflection increasing to 12.43 mm. A photograph of the failure at the slab-column connection of Specimen P150 is shown in Fig. 3.5.

The measured strains in the strain gauges in the tension reinforcement at full service load and at the peak load are shown in Figure 3.6a & 3.6b. The highest strains were recorded in the weak direction in the first reinforcing bar, 75 mm away from the center of the slab. As can be seen from Fig. 3.6b, the first reinforcing bar in the weak direction reached 2158 micro-strain at the peak load, that is just below yield level of 2325 micro-strain. As in the case of Specimen P100, strains decreased with distance from the column face.

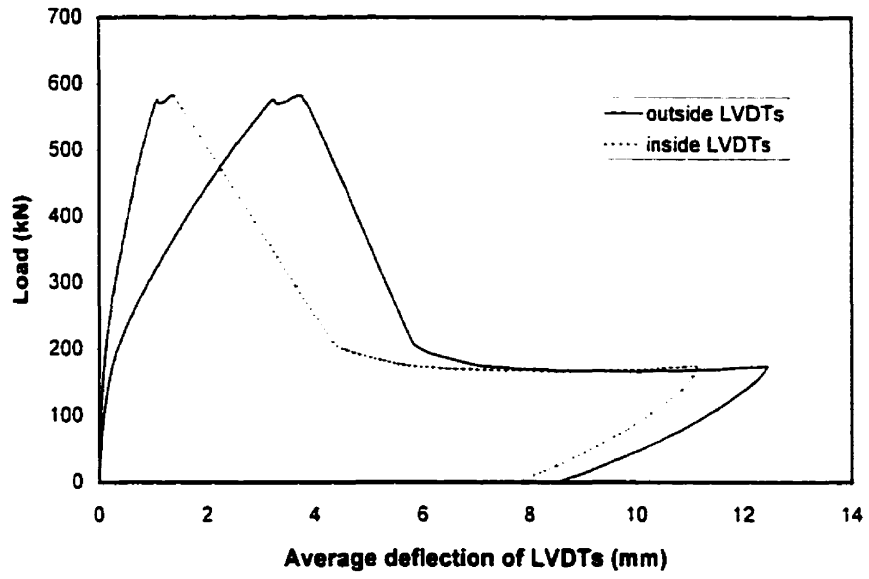


Figure 3.4 Load versus average deflection responses of Specimen P150

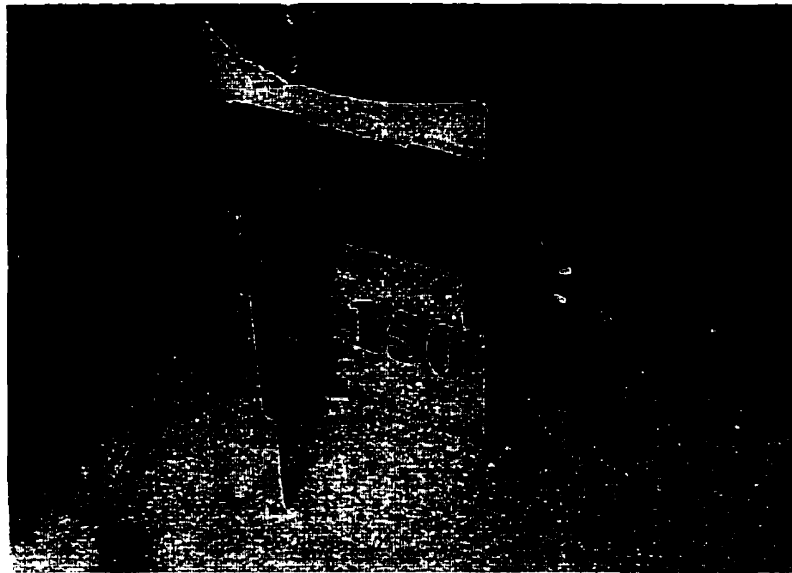
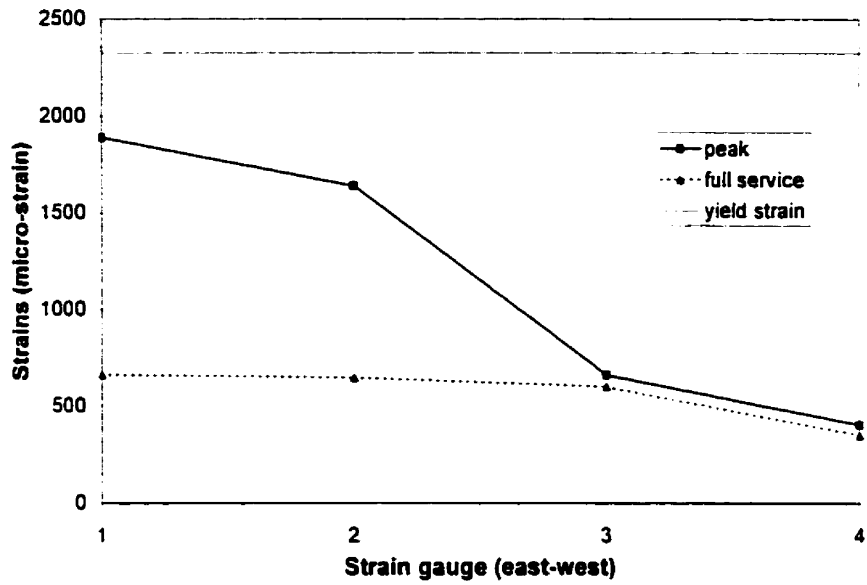
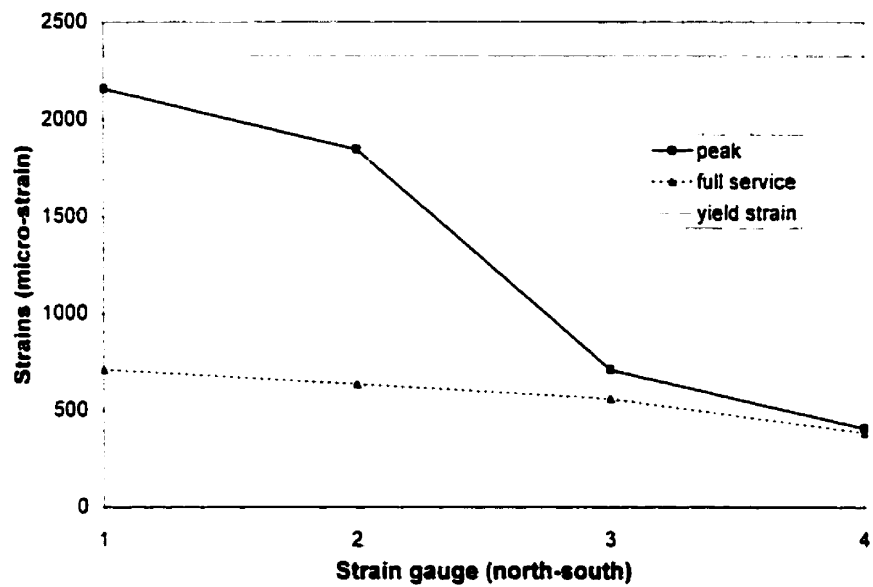


Figure 3.5 Failure at slab-column connection for Specimen P150



a) Strong direction



b) Weak direction

Figure 3.6 Strains in tension reinforcing bars at full service and peak load for Specimen P150

3.3 Specimen P200

The total load versus deflection response of Specimen P200, is shown in Fig. 3.7. As can be seen from this figure, the load-deflection curve exhibits a change in stiffness when the first crack occurs at a load of 236 kN. First yielding occurred in one of the bars in the strong direction (north-south direction) at a total load of 594 kN and a corresponding average deflection of 1.93 mm. This yielding occurred in the first reinforcing bar, 75 mm from the column face. The maximum load reached was 904 kN with a corresponding deflection of 4.23 mm, before failing abruptly in punching shear. The failure was instantaneous, with the load dropping to 375 kN and deflection increasing to 13.6 mm. A photograph of the failure of the slab column connection of Specimen P200 is shown in Fig. 3.8.

Figures 3.9a & 3.9b show the measured strains in the strain gauges in the tension reinforcement at full service load and at the peak load. The highest strains were recorded in the weak direction in the first reinforcing bar, 75 mm away from the center of the slab, and in the strong direction in the first reinforcing bar, 75 mm away from the center of the slab. As can be seen from Figure 3.9b, the first reinforcing bar in the weak direction reached 2461 micro-strain at peak load, and the first reinforcing bar in the strong direction also reached 2523 micro-strain at peak load, that is, just above the yield level of 2325 micro-strain.

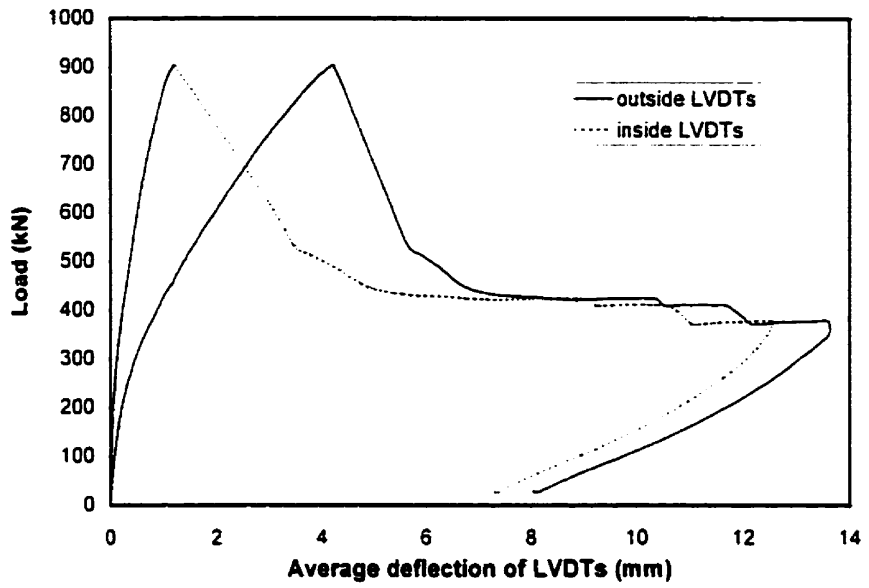
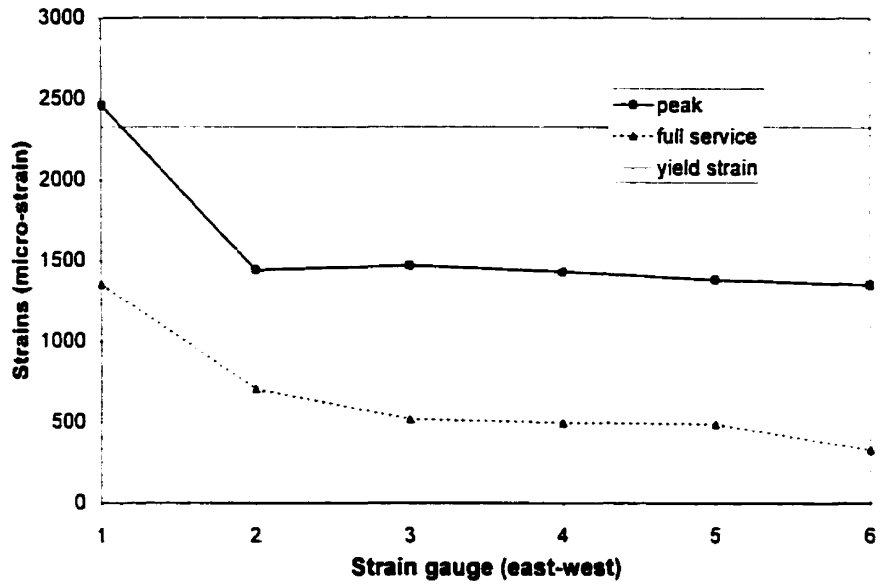


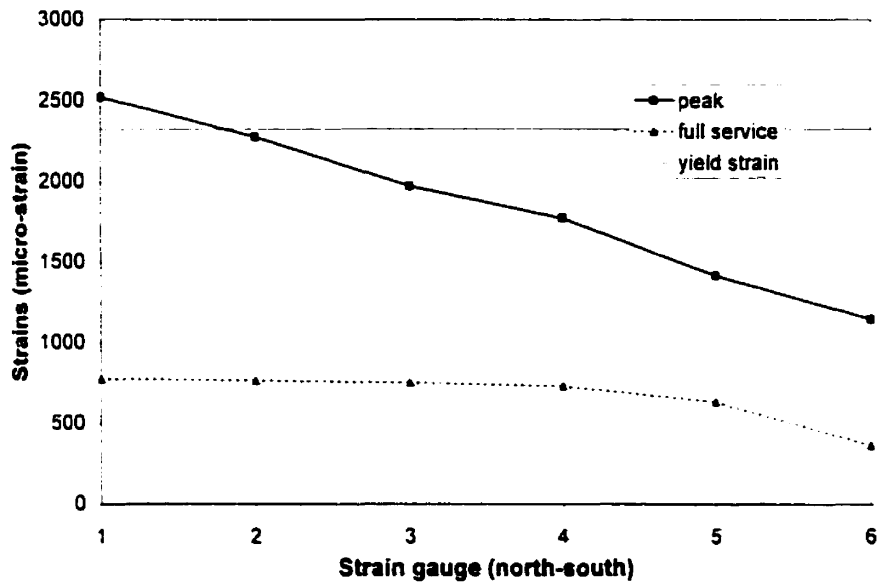
Figure 3.7 Load versus average deflection responses of Specimen P200



Figure 3.8 Failure at slab-column connection for Specimen P200



a) Strong direction



b) Weak direction

Figure 3.9 Strains in tension reinforcing bars at full service and peak load for Specimen P200

3.4 Specimen P300

The total load versus deflection response of Specimen P300 is shown in Fig. 3.10. As can be seen from this figure, the load-deflection curve exhibits a change in stiffness when first cracking occurs at a load of 442 kN. No yielding occurred in the reinforcing bars in both directions. The maximum load reached was 1381 kN with a corresponding deflection of 4.34 mm, before failing abruptly in punching shear. The failure was instantaneous, with the load dropping to 501 kN and deflection increasing to 13.44 mm. The photo of the failure of the slab column connection of Specimen P300 is shown in Figure 3.11.

Figures 3.12a & 3.12b show the measured strains in the strain gauges in the tension reinforcement at full service load and at the peak load. At the full service load and peak load, none of the bars reached yield and the reinforcing bars throughout the entire width of the slab exhibited similar strain readings. The highest strains were recorded in the weak direction in the first reinforcing bar, 130 mm away from the centre of the slab, and in the strong direction the first reinforcing bar, 130 mm from the centre of the slab. On average, the strains were higher in the strong direction. The maximum strain recorded was 1976 micro-strain, less than the yield level of 2340 micro-strain of the No.20 reinforcing bars.

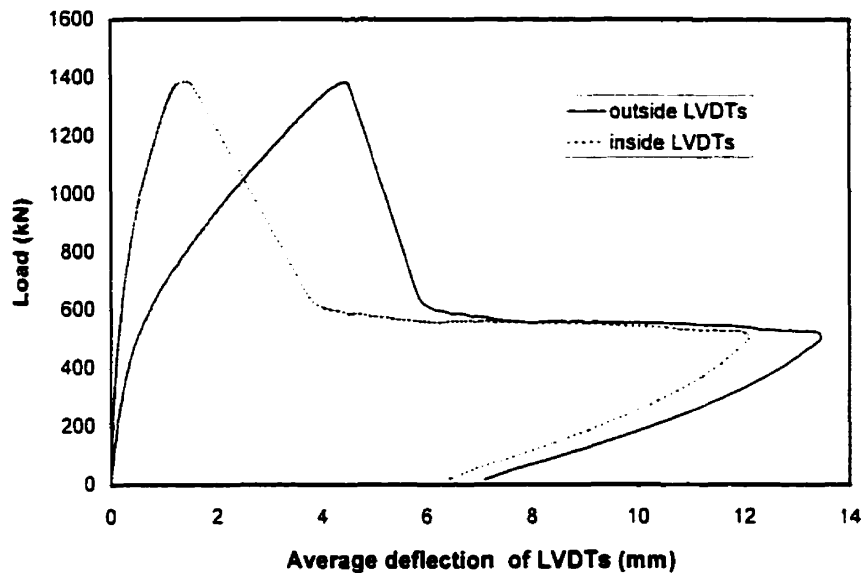


Figure 3.10 Load versus average deflection responses of Specimen P300

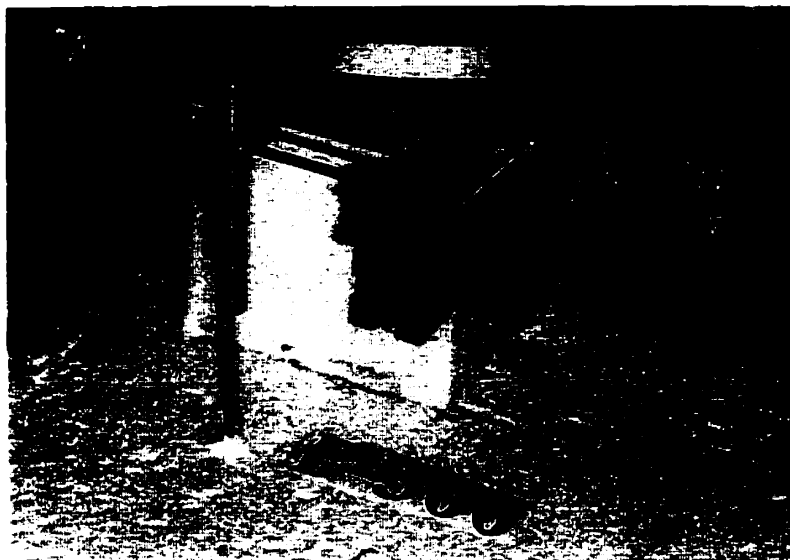
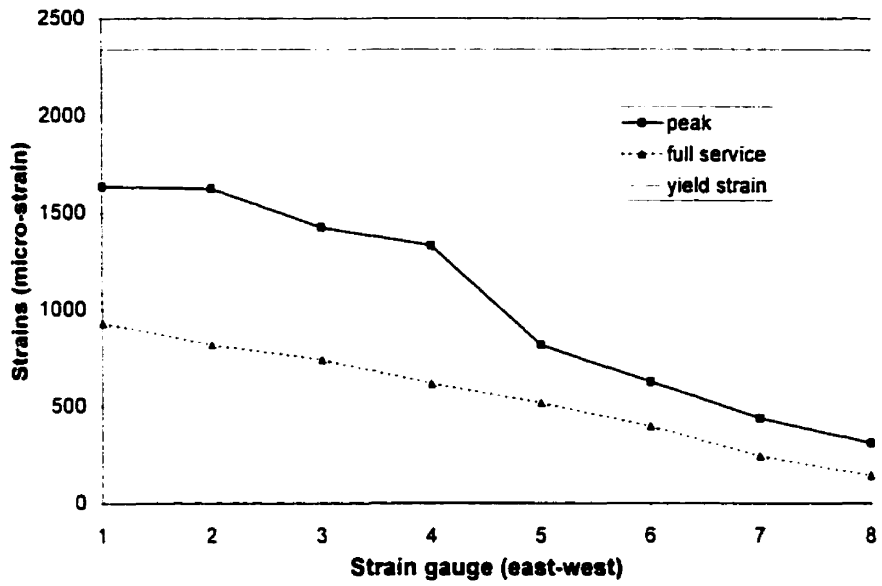
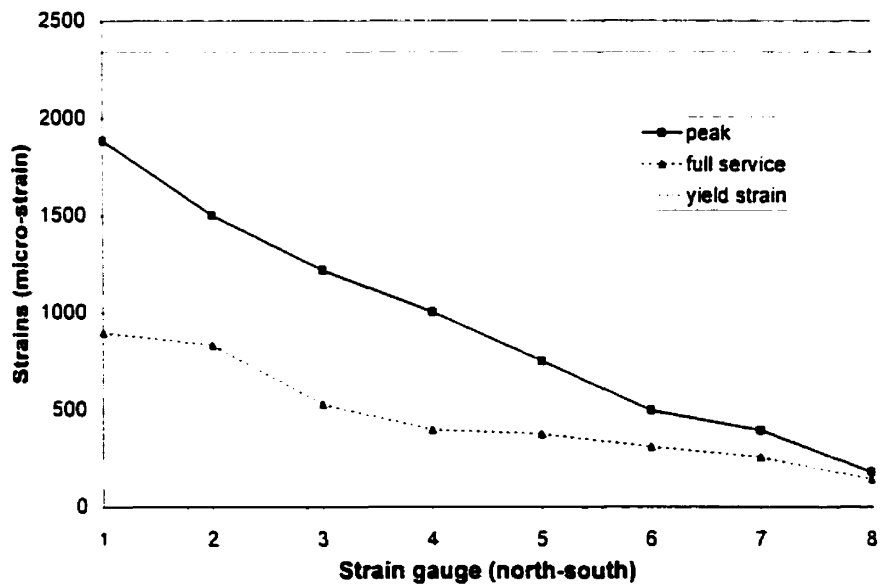


Figure 3.11 Failure at slab-column connection for Specimen P300



a) Strong direction



b) Weak direction

Figure 3.12 Strains in tension reinforcing bars at full service and peak load for Specimen P300

3.5 Specimen P400

The total load versus deflection response of Specimen P400, with a concrete strength of 39.4 MPa and a uniform distribution of the top mat of reinforcement, is shown in Fig. 3.13. As expected, the load-deflection curve was stiffer up to the point of first cracking at a load of 270 kN. The maximum load reached was 2224 kN with a corresponding deflection of 2.87 mm, before failing abruptly in punching shear. The failure was instantaneous, with the load dropping to 1033 kN and deflection increasing to 13.46 mm. A photograph of the failure of the slab column connection of Specimen P400 is shown in Fig. 3.14.

Figures 3.15a & 3.15b show the measured strains in the strain gauges in the tension reinforcement at full service load and at the peak load. At full service and peak load none of the bars reached yield and the reinforcing bars throughout the entire width of the slab exhibited similar strain readings. The highest strains were recorded in the first bar from the centerline in both the strong and weak direction. The maximum strain recorded was 1553 micro-strain, which is below the yield level of 2165 micro-strain.

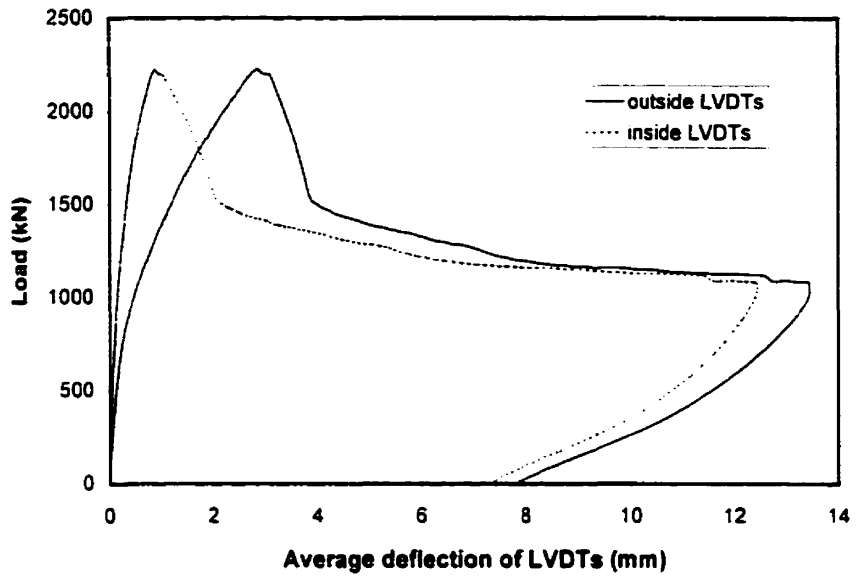


Figure 3.13 Load versus average deflection responses of Specimen P400

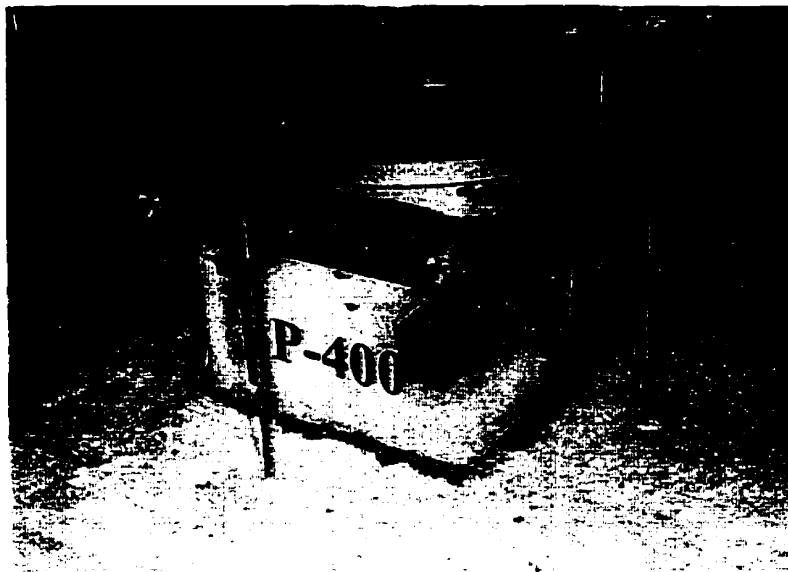
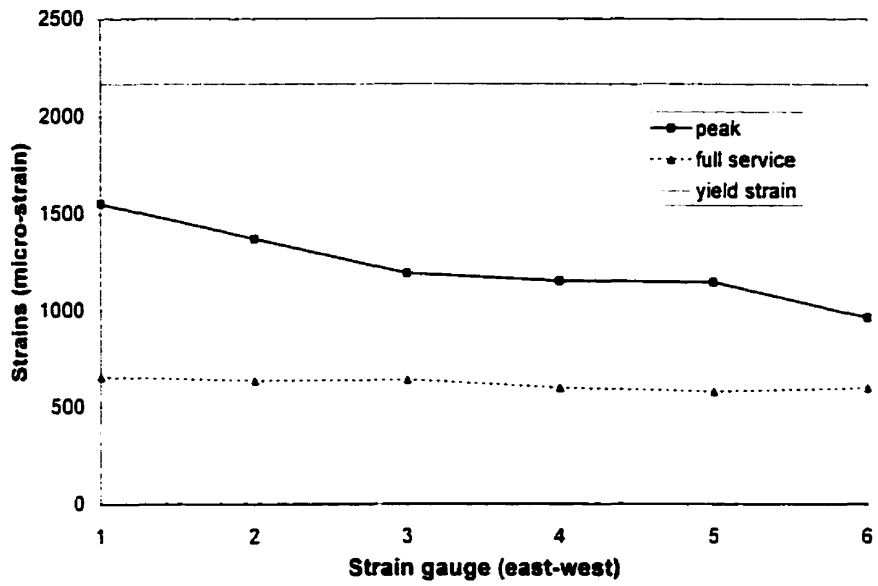
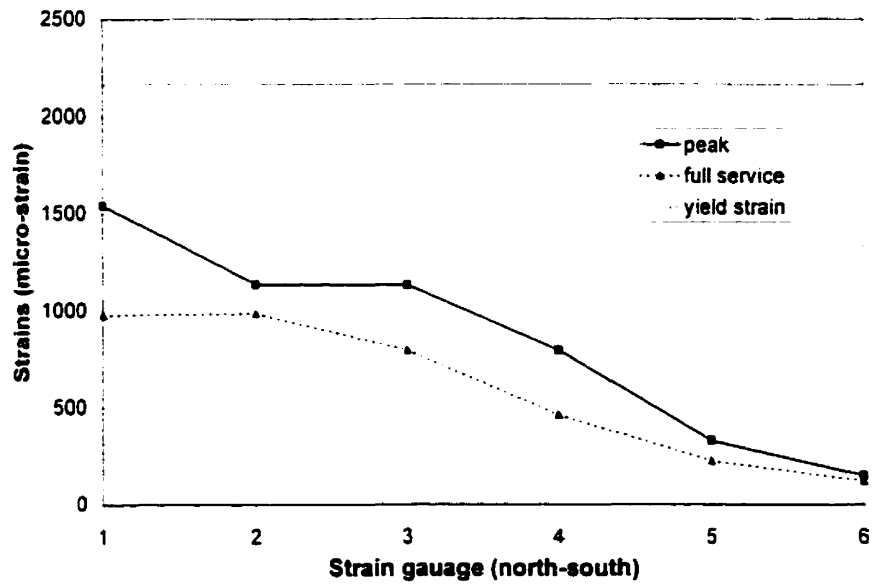


Figure 3.14 Failure at slab-column connection for Specimen P400



a) Strong direction



b) Weak direction

Figure 3.15 Strains in tension reinforcing bars at full service and peak load for Specimen P400

3.6 Specimen P500

The total load versus deflection response of Specimen P500 is shown in Fig. 3.16. As can be seen from this figure, the load-deflection curve exhibits a change in stiffness when the first crack occurs at a load of 360 kN. First yielding occurred in one of the bars in the weak direction at a total load of 1417 kN and a corresponding average deflection of 0.17 mm. This yielding occurred in the first reinforcing bar, 148 mm from the column face. The maximum load reached was 2681 kN with a corresponding deflection of 2.79 mm, before failing abruptly in punching shear. The failure was instantaneous, with the load dropping to 1007 kN and deflection increasing to 15.58 mm. Figure 3.17 shows a photograph of the failure of the slab column connection of Specimen P500.

Figures 3.18a & 3.18b show the measured strains in the strain gauges in the top mat of reinforcement at full service load and at the peak load. The first bar from the centre of the slabs in the weak direction displayed the highest strain during the test and was the only bar to have reached yield at full service load. The highest strains were recorded in the first reinforcing bar of the weak direction, 148 mm away from the center of the slab. As can be seen from Fig. 3.18, the reinforcement in the strong direction reached 1416 micro-strain at full service load, that is below the yield level of 2165 micro-strain of the No. 25 reinforcing bars. In general, strains decreased with distance from the column face.

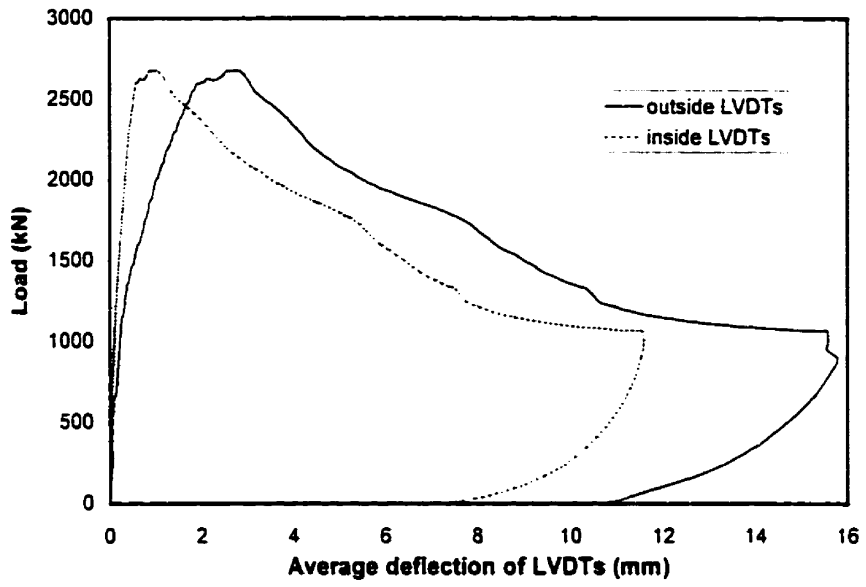
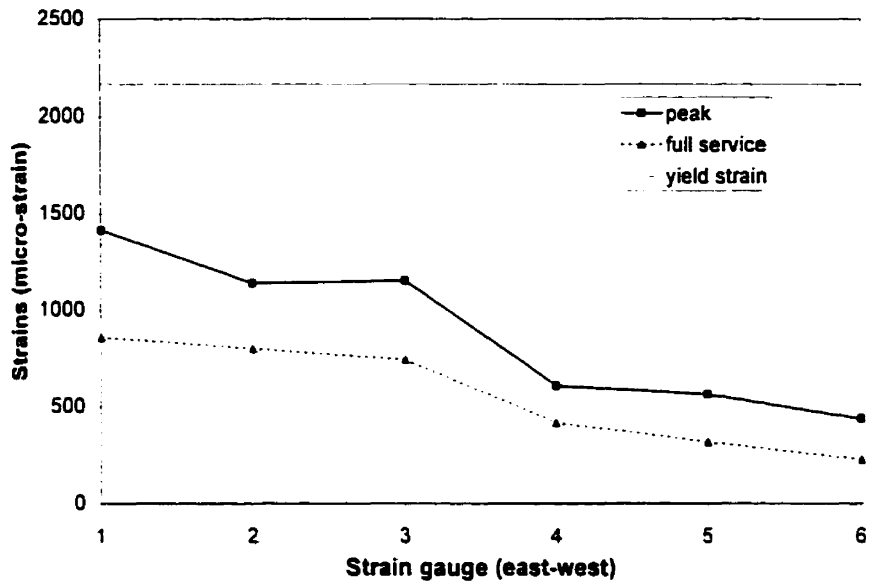


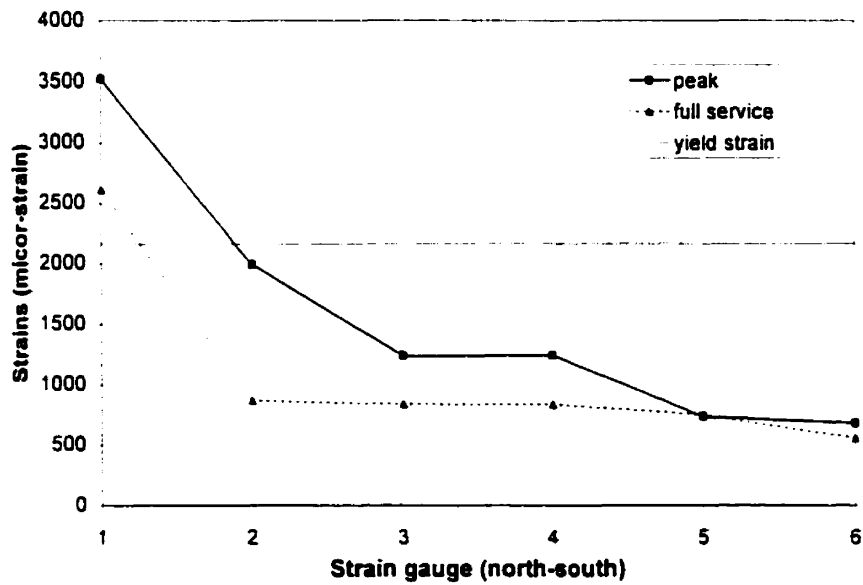
Figure 3.16 Load versus average deflection responses of Specimen P500



Figure 3.17 Failure at slab-column connection for Specimen P500



a) Strong direction



b) Weak direction

Figure 3.18 Strains in tension reinforcing bars at full service and peak load for Specimen P500

3.7 Summary of Results

Table 3.1 summarizes the test results for the six specimens giving the failure shear and the shear stress at failure, based on the CSA critical shear section. It is observed that all specimens failed in punching shear.

Table 3.1 Summary of results

Specimen	V_{max} (kN)	V/b_0d (MPa)
P100	330	2.76
P150	583	2.78
P200	904	2.83
P300	1381	2.32
P400	2224	2.00
P500	2681	1.68

Figure 3.19 shows the failure shear stress versus specimen effective depth, d . From Fig. 3.19, it can be seen that for effective depths up to 200 mm, the failure shear stress is relatively constant. For effective depth depths greater than 200 mm, the failure shear stress decreases as the effective depth of the specimen increases. Specimen P200 has the highest failure shear stress at failure, while Specimen P500 has the lowest failure shear stress. It is evident that for this test series, there is a significant size effect for effective depths greater than about 200 mm.

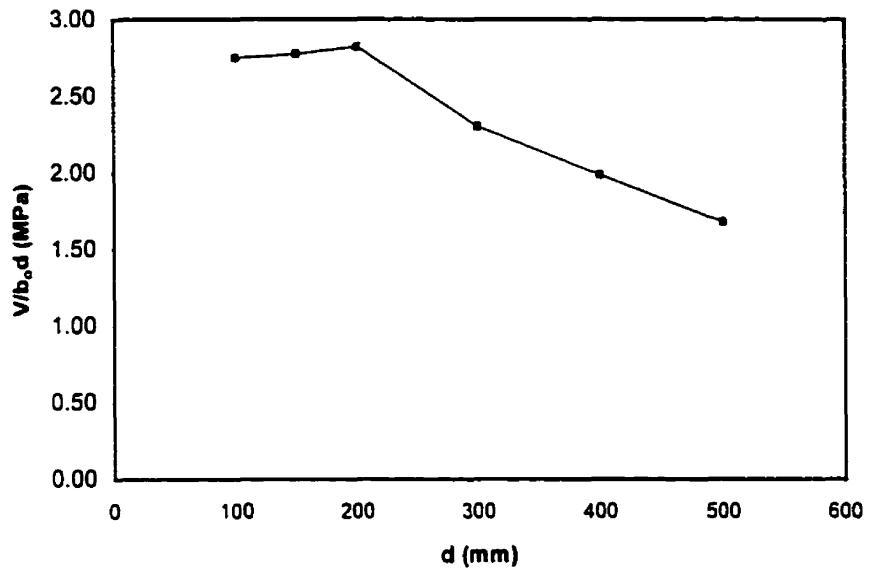


Figure 3.19 Shear stress at failure versus specimen depth

Chapter 4

Analysis of Results

4.1 Comparison of Two-Way Slab Test Results

This section compares the observed experimental behaviour of the six slab test specimens. Some of the experimental results that are compared include the load versus deflection responses of the slabs and the load versus strain distribution in the reinforcing bars.

4.1.1 Load-Deflection Responses

Table 4.1 provides the measured total loads and the average deflections at first cracking, first yielding, full service load and peak load for the slab specimens. Figures 4.1 and 4.2 compare the total load versus average deflection responses of the six slab test specimens.

From Table 4.1, it can be seen that the first cracking loads increased with the increase in the effective depth of the slab test specimen. Specimen P100 exhibited the smallest first cracking loads while Specimen P500 exhibited the highest loads. It is interesting to note that the first cracks in the slab specimens started at the corners of the column where the stresses were the highest and then the cracks propagated towards the edges of the slab. The peak loads for the test specimens ranged from 330 kN for Specimen P100 to 2681 kN for Specimen P500.

All the slabs exhibited an abrupt shear mode of failure. The specimens failed along inclined surfaces extending out from the compression zone at the column face to some distance away from the column face. After the peak loads were reached, all of the loads dropped instantaneously to approximately one-half of the load carrying capacities

of the slab specimens. Only Specimens P200 and P500 experienced some yielding of the tension reinforcement before failing in punching shear.

Table 4.1 Summary of key loads and deflections for slab test specimens

Specimen		First Cracking	Full Service Load	First Yielding	Peak Load
P100	load (kN)	61	149	no	330
	deflection (mm)	0.08	0.44	yielding	2.64
P150	load (kN)	154	261	no	583
	deflection (mm)	0.20	0.67	yielding	3.75
P200	load (kN)	236	398	594	904
	deflection (mm)	0.28	0.86	1.93	4.23
P300	load (kN)	242	746	no	1381
	deflection (mm)	0.39	1.20	yielding	4.43
P400	load (kN)	270	1392	no	2224
	deflection (mm)	0.28	1.00	yielding	2.87
P500	load (kN)	360	1989	1417	2681
	deflection (mm)	0.04	1.00	0.44	2.79

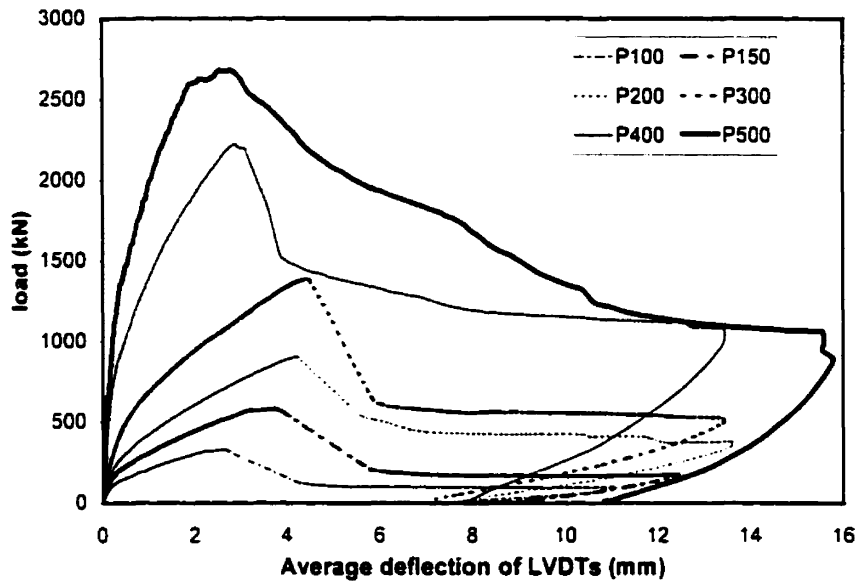


Figure 4.1 Comparison of load versus average deflection responses of the outer LVDTs for the six slab specimens

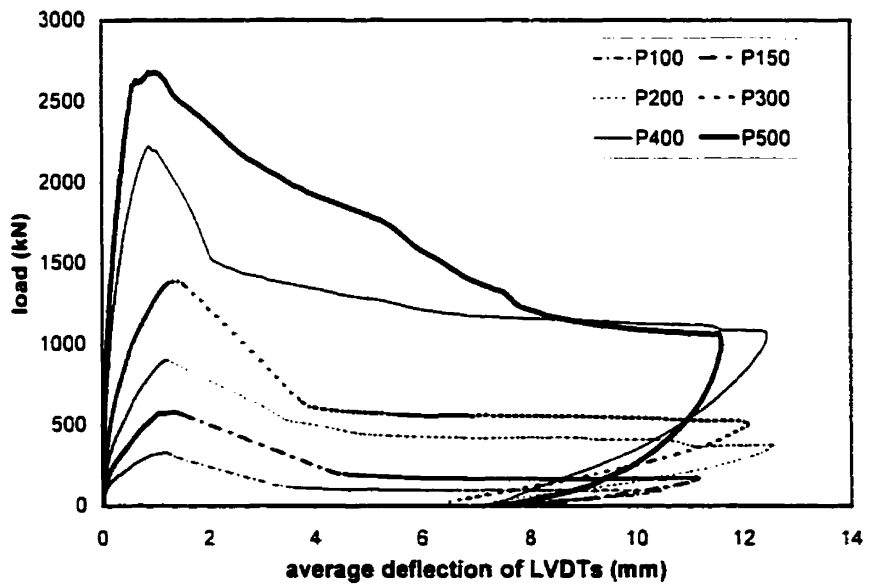


Figure 4.2 Comparison of load versus average deflection responses of the inner LVDTs for the six slab specimens

4.1.2 Strain Distributions of Reinforcing Steel

Tables 4.2 and 4.3 show the strain distributions recorded for the flexural tension reinforcement in the strong and weak directions at the full service and peak load for the test specimens. The six specimens had very similar strain distributions. As expected, the reinforcement exhibited higher strains near the column. Due to the two-way action in slabs, the slab moments are higher at the column face due to the larger stiffness of this region.

Table 4.2 Strain distributions in the strong and weak directions at full service load

Strains in the Strong Direction at Full Service Load (micro-strain)								
	1	2	3	4	5	6	7	8
P100	505	501	245	233	-	-	-	-
P150	663	647	601	351	-	-	-	-
P200	1354	704	517	495	488	331	-	-
P300	932	818	743	618	518	397	245	144
P400	657	637	642	600	581	600	-	-
P500	860	800	743	417	319	228	-	-

Strains in the Weak Direction at Full Service Load (micro-strain)								
	1	2	3	4	5	6	7	8
P100	281	254	216	133	-	-	-	-
P150	712	636	560	584			-	-
P200	777	766	753	733	635	365	-	-
P300	898	832	530	397	377	312	259	144
P400	980	988	796	463	227	123	-	-
P500	2611	868	841	838	752	557	-	-

Table 4.3 Strain distributions in the strong and weak directions at peak load

Strains in the Strong Direction at Peak Load (micro-strain)								
	1	2	3	4	5	6	7	8
P100	2033	1318	610	443	-	-	-	-
P150	1891	1641	662	405	-	-	-	-
P200	2461	1442	1471	1432	1382	1350	-	-
P300	932	818	743	618	518	397	245	144
P400	1553	1372	1193	1154	1147	965	-	-
P500	1416	1139	1152	608	564	438	-	-

Strains in the Weak Direction at Peak Load (micro-strain)								
	1	2	3	4	5	6	7	8
P100	1802	686	667	636	-	-	-	-
P150	2158	1846	710	407	-	-	-	-
P200	2523	2275	1972	1775	1416	1147	-	-
P300	1886	1501	1219	1003	751	497	395	180
P400	1542	1136	1133	796	331	150	-	-
P500	3524	1992	1236	1243	735	681	-	-

4.2 Comparison of Predictions with Failure Loads

The experimental results obtained for the punching shear strength of the slab specimens will be compared to the predicted failure loads using different code equations in this section. Table 4.4 summarizes the nominal punching shear strength capacities for the six test specimens as predicted by the CSA Standard (1994), the BS Standard (1985) and the CEB-FIP Model Code (1990). All of the code expressions used to determine the values in Table 4.4 are given in Table 1.1. Figure 4.3 shows the comparison between the experimentally determined failure loads and the failure loads predicted using the three different expressions. Figure 4.4 compares the failure shear stress to the code predictions for the slab specimens. It must be noted that the punching shear stresses reported in Fig. 4.4 were obtained by dividing the punching shear capacity, V , by the area of the CSA critical shear section, b_0d . This approach was necessary because the expressions for the punching shear strength in the CEB-FIP Model Code and the BS Standard are based on different critical sections than that assumed by the CSA Standard.

Table 4.4 Comparison of failure loads to code predictions for slab specimens

Specimen	f'_c (MPa)	ρ (%)	Shear Resistance (kN)			
			Experimental Results	CSA Standard (1994)	BS 8110 (1995)	CEB-FIP (1990)
P100	39.4	0.97	330	249	342	268
P150	39.4	0.90	583	435	587	456
P200	39.4	0.83	904	663	873	677
P300	39.4	0.76	1381	1243	1581	1237
P400	39.4	0.76	2224	2320	2676	2112
P500	39.4	0.76	2681	3314	4013	3034

The punching shear strength expression of the CSA Standard do not include a size effect term. As can be seen from Fig. 4.4 and from Table 4.4, the lack of a size factor in the code equations leads to unconservative predictions for the slabs with effective depths greater than 300 mm. The expressions for the punching shear strength of the BS Standard

and the CEB-FIP Model Code both include a size effect term in their calculations of the shear resistance. The BS Standard has a size factor of $\sqrt[3]{400 / d}$, which should not be taken as less than 1. In the other words, the shear stress resistance is reduced up to an effective depth, d , of 400 mm, after which the shear stress resistance becomes constant with increasing d . The CEB-FIP Model Code has a size factor of $1 + \sqrt{200 / d}$. As can be seen from Table 4.4 and Figs. 4.3 and 4.4, the BS Standard gives conservative predictions of the punching shear strength, except for slabs with effective depths greater than about 300 mm. The CEB-FIP Model Code expression is also conservative as it results in shear strength values that are smaller than the experimental results recorded for the punching shear strength of all but one of the slab test specimens (P500).

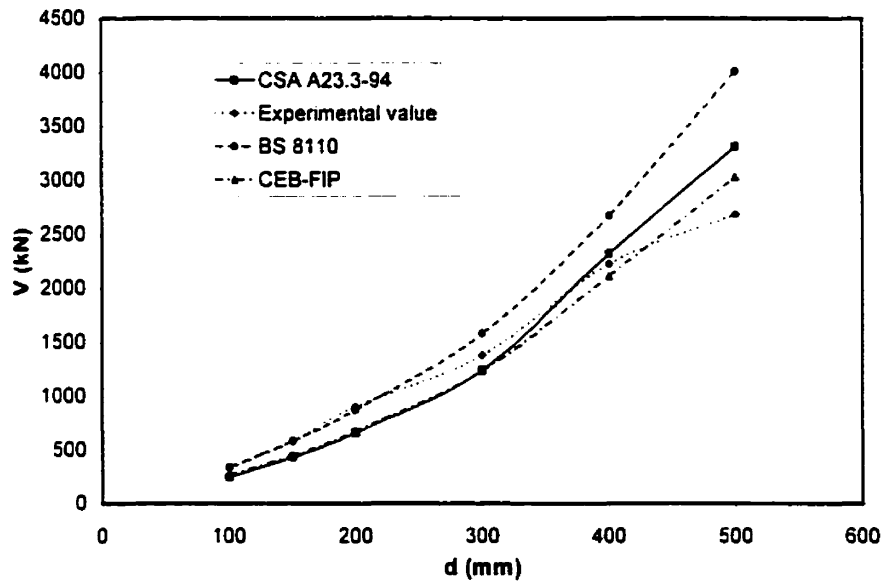


Figure 4.3 Comparison of experimental and predicted failure loads

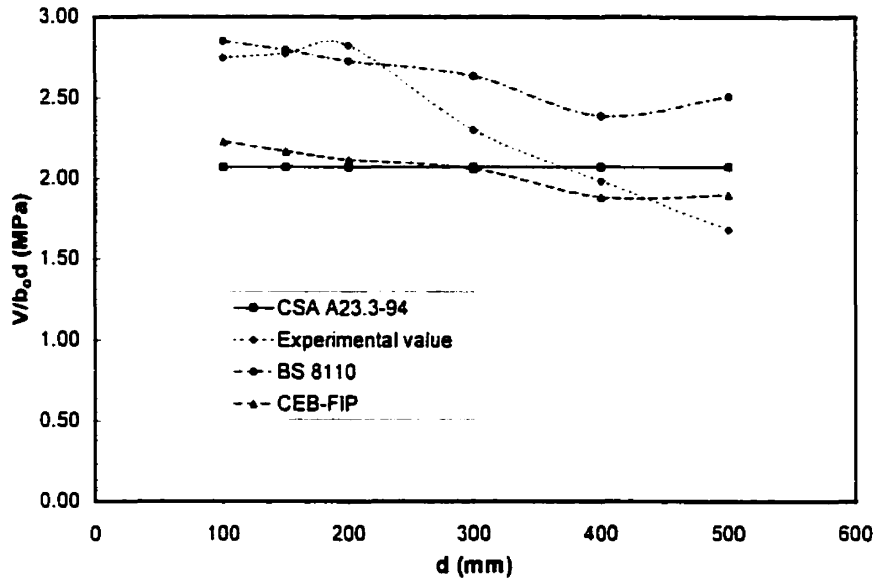


Figure 4.4 Comparison of experimental and predicted failure stress

For one way beam shear, the CSA Standard reduces the shear resistance of $0.2\phi_c\sqrt{f'_c}$ for $d > 300$ mm using a size reduction factor of $1300/(1000+d)$ which should not be taken as less than 0.5. A comparison of the size reduction factors of the CSA Standard, the BS Standard and the CEB-FIP Model Code is given in Fig 4.5. For the modified CSA Standard expression, the size reduction factor is for one way shear, while the size reduction factors of the BS Standard and the CEB-FIP Model Code are for two-way punching shear. For the CEB-FIP Model Code expression, the size effect was taken as $((1 + \sqrt{200/d})/2)$ such that for $d = 200$ mm, the size reduction factor is 1.0. From Fig 4.5, it is clear that the size effect expression of the CSA Standard for one-way shear is very similar to the expression in the CEB-FIP Model Code. Both of these expressions for the size effect are more conservative than the size effect expression of the BS Standard. Figure 4.6 compares the experimental result and the punching shear strength expression of the CSA Standard with and without using the size reduction factor. It can be seen that when the size reduction factor is used, the CSA Standard gives conservative predictions for the slabs with effective depth less than 400 mm. In addition, the expression also gives more realistic prediction of the shear capacity for Specimen P500. Thus, it is

recommended to include the size reduction factor of $1300/(1000+d)$ into the CSA Standard expression for the punching shear strength.

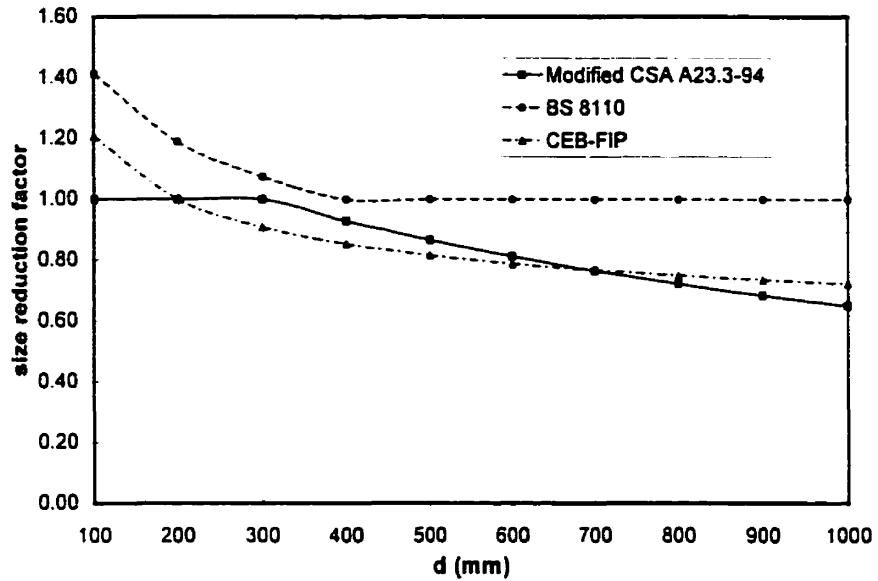


Figure 4.5 Comparison of the size reduction factors according to different codes

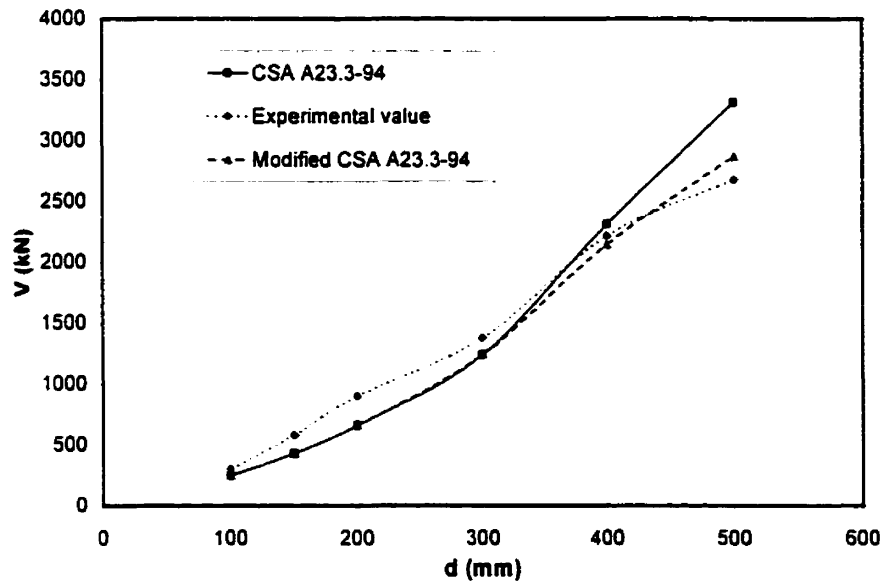


Figure 4.6 Comparison of experimental results and CSA Standard modified with size reduction factor of one way shear

Table 4.5 provides a summary of the nominal punching shear strength values for the six test specimens as predicted by Rankin *et al.* (1987), Gardner *et al.* (1996) and Sherif *et al.* (1996). The equations used to evaluate the punching shear strengths in Table 4.5 can be found in Chapter 1 (see Equations 1.7, 1.8 and 1.9).

Table 4.5 Comparison of failure loads to predictions using equations proposed by various investigators

Specimen	f'_c (MPa)	ρ (%)	Shear Resistance (kN)			
			Experimental Results	Rankin et al. (1987)	Gardner et al. (1996)	Sherif et al. (1996)
P100	39.4	0.97	330	310	271	283
P150	39.4	0.90	583	532	454	482
P200	39.4	0.83	904	795	674	716
P300	39.4	0.76	1381	1459	1231	1304
P400	39.4	0.76	2224	2724	2073	2260
P500	39.4	0.76	2681	3891	2992	3014

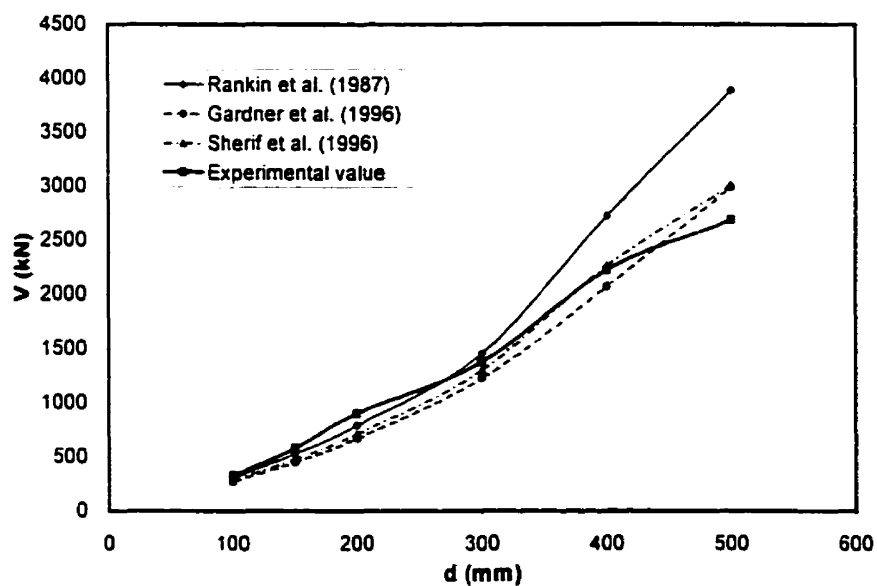


Figure 4.7 Comparison of experimental results and predicted failure loads by various investigators

Rankin *et al.* (1987) proposed Equation 1.7 for the punching shear strength of slabs. In their expression, the shear stress is assumed to be a function of the square root of the concrete compressive strength and a function of $\sqrt[3]{\rho}$. As can be seen from Table 4.5 and Fig. 4.7, the use of Equation 1.7 results in shear strength predictions that are significantly higher than the experimental results obtained for the slab test specimens with effective depths, d , greater than 300 mm.

Gardner *et al.* (1996) suggested that the punching shear load is approximately proportional to the cube root of the concrete strength, steel ratio and steel yield stress. They proposed Equation 1.8 for the shear strength of slabs. From Table 4.5 and Fig. 4.7, it can be seen that, except for Specimen P500, Equation 1.8 conservatively predicts the shear strength of the slab specimens.

Sherif *et al.* (1996) proposed Equation 1.9 for the shear strength of slabs. In this equation, the shear strength is assumed to be a function of the cube root of both the concrete compressive strength and the steel reinforcement ratio. It can be seen from Table 4.5 and Fig. 4.7 that, except for Specimen P400 and P500, Equation 1.9 conservatively predicts the shear strength of the slab specimens.

4.3 Predictions Using the Modified Compression Field Theory

The program Response 2000[®] developed at the University of Toronto by Micheal P. Collins and Evan C. Bentz (Collins and Bentz, 1998) was used to obtain predictions according to the modified compression field theory. This program uses a sectional analysis method that assumes that plane sections remain plane, combined with a dual-section analysis and the modified compression field theory to determine shear response.

It is important to realize that for small shear span-to-depth ratios, a/d , sectional analysis may not be appropriate. For small a/d ratios, the applied load is close to the support and this causes a disturbance in the flow of stresses. There is a tendency for the forces to flow from the point of application of the load, directly into the support reaction. This "strut action" creates a "disturbed region" in which the assumptions of plane section and of uniformly distributed shear stresses are inappropriate. The behaviour of Specimen P500 may have been influenced by the relative small a/d of 1.48 and hence may have a higher failure load than if it had a larger a/d ratio

In order to predict the results, the slab was modeled as four beams framing into the column. These beams have a width equal to the column width at the column face and a variable width away from the column face. It is assumed that the width spreads at an angle of 45° . For the predictions using Response 2000[®], the locations chosen for the sectional analyses were taken at a distance equal to the effective depth, d from the face of column and at $d/2$ from the face of the column. This is to see what predictions result for these two critical sections, subjected to differing shear and moment. The measured material properties were used for the predictions, as well as, the "as-built" cross-sectional dimensions. The input and output values for each specimen are presented in Appendix A and the results obtained from Response 2000[®] are summarized in Table 4.6 and Figs.4.8 and 4.9.

Table 4.6 Modified compression field theory predictions by Response 2000^e

Specimen	Experimental Results (kN)	Response 2000 Results at d (kN)	Response 2000 Results at d/2 (kN)
P100	303	215	170
P150	583	344	261
P200	904	511	374
P300	1381	928	681
P400	2224	1972	1250
P500	2681	3466	1708

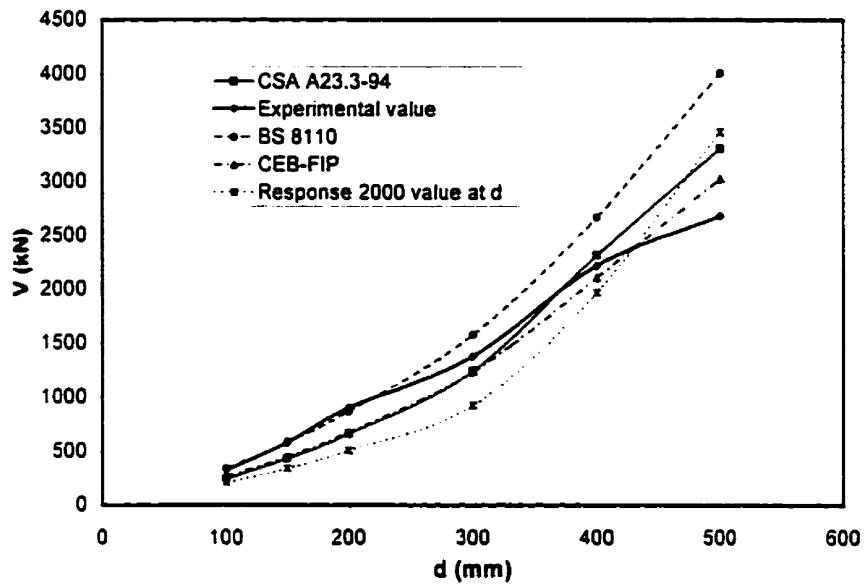


Figure 4.8 Response 2000^c predictions for distance d from the column face

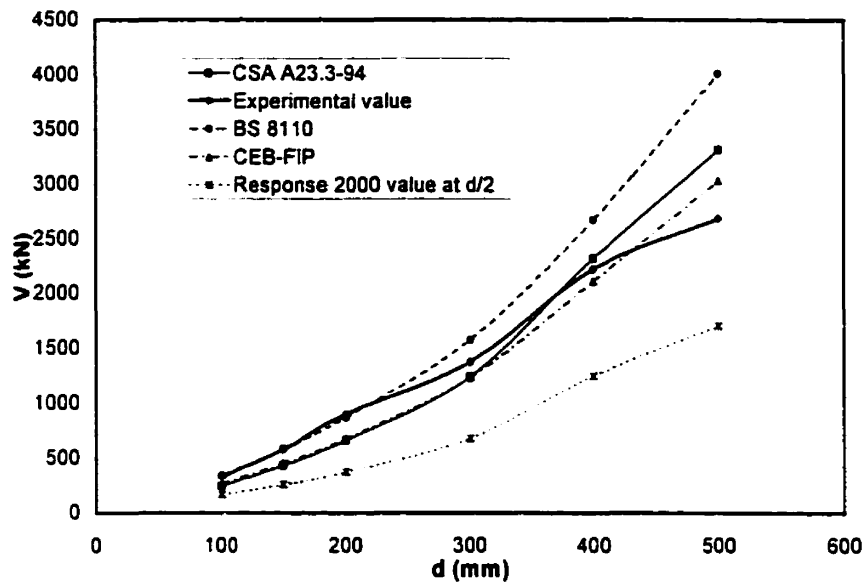


Figure 4.9 Response 2000[®] predictions for distance $d/2$ from the column face

The prediction at a distance d from the face of the column gives higher shear strength than that predicted using distance $d/2$ from the column face. When these Response 2000[®] predictions are compared with the test results, it can be seen from Table 4.6 that the predictions are very conservative, particularly the predictions for section at $d/2$ from the column face. For $d = 500$ mm, the Response 2000[®] prediction for section at d from the column face is unconservative and has a predicted shear strength which is almost 27% larger than the experimental value. When compared to the code predictions, the Response 2000[®] predictions for section at d from the column face has a similar trend to the ACI Code and CSA Standard value as shown in Fig 4.8. The predicted shear strength values for both sections are very conservative. When compared to the BS Standard and the CEB-FIP Model Code, the Response 2000[®] predictions are very conservative and significantly smaller than the code predictions.

Chapter 5

Conclusions

5.1 Conclusions of this Experimental Program

The following conclusions were drawn from the results of the experimental program on the six two-way slab specimens:

1. It is observed that all the specimens failed in punching shear.
2. It is evident that for this test series, there is a significant size effect for effective depths greater than about 200 mm.
3. The CSA Standard (1994) expressions result in conservative predictions of the punching shear strength, except for the slabs with effective depth greater than 300 mm. The BS Standard gives conservative predictions of the punching shear strength, except for slab with effective depths greater than about of 300 mm. The CEB-FIP Model Code expression is conservative except for slabs with effective depth greater than 400 mm.
4. The CSA A23.3-94 Standard expressions for the punching shear strength of interior slab-column connections should be modified to take into account the effect that the size effect has on the punching shear strength of slabs. The size reduction factor of $1300/(1000+d)$ used for one way shear in the CSA Standard results in better predictions of the experimental results.
5. The punching shear strength expressions proposed by Gardner *et al.* and Sherif *et al.* both overestimate the punching shear capacity of Specimen P500. The equation proposed by Rankin *et al.* for computing the shear strength of slabs results in very unconservative strength predictions for specimens with effective depth greater than 300 mm.

6. The modified compression field theory which accounts for the size effect, moment-to-shear ratio, and amount of reinforcement gives overly conservative predictions at a distance $d/2$ from the column face, but more realistic predictions of the shear capacity, if the critical section is taken at d from the column face. The predictions are conservative for effective depths up to and including 400 mm, but unconservative for an effective depth equal to 500 mm.

It is hoped that the results obtained from this experimental program will help other research efforts in better understanding the “size effect” affecting punching shear in concrete. It is hoped as well that the experimental data obtained will be use to researchers working towards a more accurate prediction of the punching shear strength of two-way slabs

References

CODES

American Concrete Institute (ACI) 1989. Building Code Requirements for Reinforced Concrete and Commentary (ACI 318-89 and ACI 318R-89). Detroit, Michigan, 353 pp.

American Concrete Institute (ACI) 1995. Building Code Requirements for Reinforced Concrete and Commentary (ACI 318-95 and ACI 318R-95). Detroit, Michigan, 369 pp.

Canadian Standards Association (CSA) 1984. CSA A23.3-M84. Code for the Design of Concrete Structures for Buildings. CSA, Rexdale, Ontario, 281 pp.

Canadian Standards Association (CSA) 1994. CSA A23.3-94. Design of Concrete Structures. CSA, Rexdale, Ontario, 220 pp.

Comité Euro-International du Béton et Fédération Internationale de la Précontrainte (CEB-FIP) 1990. Model Code for Concrete Structures (MC90 model code). Lausanne, Switzerland.

British Standard Institution (BSI) 1985. Structural Use of Concrete (Standard BS-8110). London, United Kingdom.

Associate Committee on the National Building Code (NBC) 1995. National Building Code of Canada 1995 (NBCC). National Research Council of Canada, Ottawa, 571 pp.

American Association of State Highway and Transportation Officials 1994. AASHTO LRDF Bridge Design Specification and Commentary, First Edition. AASHTO, Washington, D.C., 1091pp.

ACI / ASCE

ACI-ASCE Committee 426. 1974. "The Shear Strength of Reinforced Concrete Members-Slabs". Proceedings, ASCE, V. 100, ST8, August, pp. 1543-1591.

ACI-ASCE Committee 426. 1977. "Suggested Revisions to Shear Provisions for Building Codes". Journal of the American Concrete Institute, Proceedings, V. 74, No. 9, September, pp. 458-468.

ACI-ASCE Committee 352. 1988. "Recommendations for Design of Slab-Column Connections in Monolithic Reinforced Concrete Structures", Journal of the American Concrete Institute, V. 85, No. 6, November-December, pp. 675-696.

OTHER REFERENCES

- Alexander, S.D.B. and Simmonds S.H. 1988. "Shear-Moment Interaction of Slab-Column Connections". Canadian Journal of Civil Engineering, V. 15. March, pp. 828-833.
- Alexander, S. D. B., Simmonds, S. H. 1992 "Punching Shear Tests of Concrete Slab-Column Joints Containing Fiber Reinforcement", ACI Structural Journal, V. 89, No. 4, July-Aug., pp. 425-432.
- Alexander, S.D.B. and Simmonds S.H. 1992. "Tests of Column-Flat Plate Connections". ACI Structural Journal, V. 89, No. 5, September-October, pp. 495-502.
- Bazant, Z.P. and Kazemi, M.T. 1991. "Size Effect on Diagonal Shear Failure of Beams Without Stirrups", ACI Journal, V. 88, No. 3, May-June, pp. 268-276.
- Bazant, Z.P. and Kim, Jin-Keun. 1984. "Size Effect in Shear Failure of Longitudinally Reinforced Beams". ACI Journal, V. 81, September-October, pp. 456-468.
- Collins, M.P., Bentz, E.C. 2000. "Response 2000. Reinforced Concrete Sectional Analysis Using the Modified Compression Field Theory". Version 1.0.0 (beta). University of Toronto, Toronto, Ont.
- Collins, M.P., Mitchell, D. 1997, "Prestressed Concrete Structures". Response Publications, Canada. 766 pp.
- Collins, M.P., Mitchell, D., Adebar, A., and Vecchio, F.J. 1996. "A General Shear Design Method". ACI Structural Journal, V. 93 No.1, January-February, pp. 36-45.
- Collins, M.P., Mitchell, D., and MacGregor, J.G. 1993. "Structural Design Considerations for High-Strength Concrete". Concrete International, May, pp. 27-34.
- Comité Euro-International du Béton et Fédération Internationale de la Précontrainte (CEB-FIP) 1999. Structural Concrete - the Textbook on Behaviour, Design and Performance Volume 2. Lausanne, Switzerland, 1999. 223pp.
- Elstner, R.C. and Hognestad, E. 1956. "Shearing Strength of Reinforced Concrete Slabs". Journal of the American Concrete Institute, V. 53, No.1, July, pp. 29-58.
- Gardner, N.J. and Shao, X. 1996. "Punching Shear of Continuous Flat Reinforced Concrete Slabs". ACI Structural Journal, V. 93, No. 2, March-April, pp. 218-228.
- Graf, O. 1933. "Tests of Reinforced Concrete Slabs Under Concentrated Loads Applied Near One Support". (In German), Deutscher Ausschuss für Eisenbeton, Berlin, Heft 73, 2 pages.

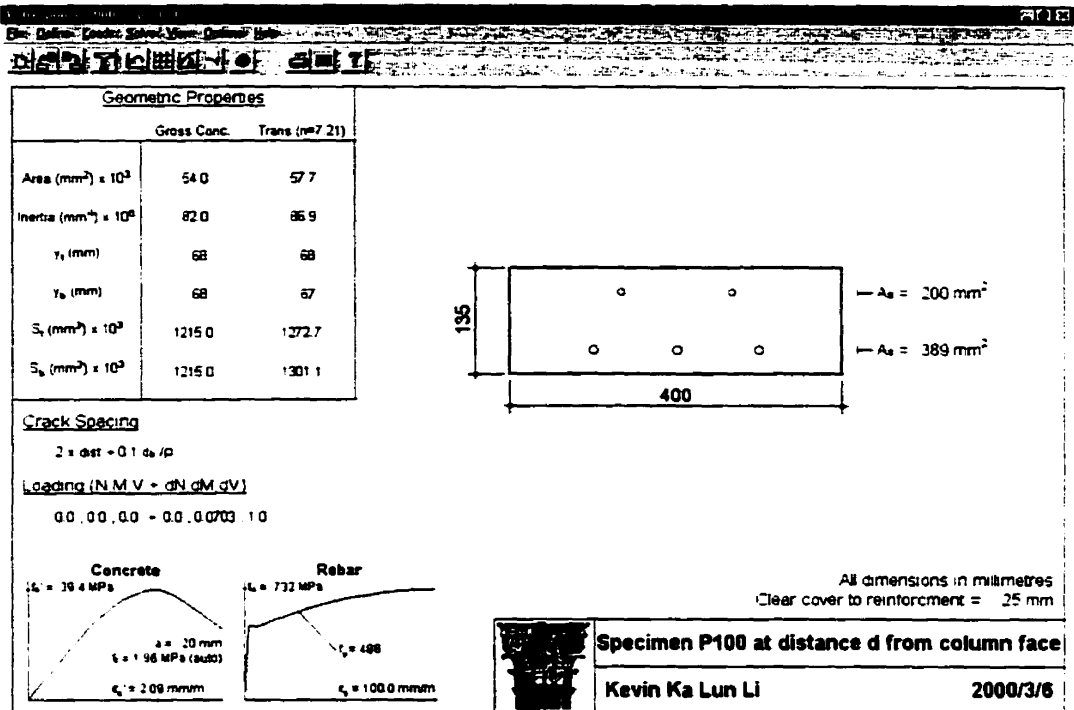
- Graf, O. 1938. "Strength Tests of Thick Reinforced Concrete Slabs Supported on All Sides Under Concentrated Loads", Deutscher Ausschuss für Eisenbeton, No. 88, Berlin, Germany.
- Hawkins, N.M and Mitchell, D. 1979. "Progressive Collapse of Flat Plate Structures". Journal of the American Concrete Institute, Proceedings V.76, No. 7, July, pp. 775-808.
- Joint Committee of 1924. 1924. "Standard Specification for Concrete and Reinforced Concrete. Joint Committee", Proceedings. American Society for Testing Materials, 24. Part I, pp. 312-385.
- Kani, G.N.J. 1966. "Basic Facts Concerning Shear Failure", ACI Journal, V. 63, June 1966, pp. 675-692.
- Kani, G.N.J. 1967. "How Safe are Our Large Reinforced Concrete Beams?", ACI Journal, V. 64, March 1967, pp. 128-141.
- Kani, M., et al. 1979. "Kani on Shear in Reinforced Concrete", University of Toronto Press, Toronto, Ontario, 1979, 225 pp.
- Kinnunen, S. and Nylander, H. 1960. "Punching of Concrete Slabs Without Shear Reinforcement". Transactions of the Royal Institute of Technology, Stockholm, No. 158, March, 112 pp.
- Marzouk, H.M. and Hussein, A. 1991 b. "Punching Shear Analysis of Reinforced High-Strength Concrete Slabs", Canadian Journal of Civil Engineering, V. 18, No. 6, pp. 954-963.
- Moe, J. 1961. "Shearing Strength of Reinforced Concrete Slabs and Footings Under Concentrated Loads". Development Department Bulletin D47, Portland Cement Association, Skokie, Ill., April, 130 pp.
- Rankin, G.I.B. and Long, A.E. 1987. "Predicting the Punching Strength of Conventional Slab-Column Specimens". Proceedings of the Institution of Civil Engineers (London), V. 82, Part 1, April, pp. 327-346.
- Regan, P.E. 1971. "Behaviour of Reinforced and Prestressed Concrete Subject to Shear Forces". Paper 7441S, Proceedings of the Institution of Civil engineers, V. 50, London, England, December, p. 522. Supplement (xvii), pp. 337-364.
- Regan, P.E. 1974. "Design for Punching Shear", Structural Engineer (London), V. 52, No. 6, pp. 197-207.
- Regan, P.E. and Braestrup, M.W. 1985. "Punching Shear in Reinforced Concrete: A State of Art Report". Bulletin D'information No. 168, Comité Euro-International de Béton, Lausanne, 232 pp.

- Regan, P.E. 1986. "Symmetric Punching of Reinforced Concrete Slabs", Magazine of Concrete Research. V. 38, No.136, September, pp. 115-128.
- Richart, F.E. 1948. "Reinforced Concrete Wall and Column Footings", Journal of the American Concrete Institute, October and November, Proc. V. 45, No. 2 and 3, pp. 97-127 and 237-260.
- Shehata, I.M. and Regan, P. 1989. "Punching in Reinforced Concrete Slabs", ASCE Journal of the Structural Division, V. 115, ST7, pp. 1726-1740.
- Sherif, A.G. and Dilger, W.H. 1996. "Critical Review of the CSA A23.3-94 Punching Shear Strength Provisions for Interior Columns", Canadian Journal of Civil Engineering, V. 23, No. 5, October, pp. 998-1101.
- Shioya, T. 1989. "Shear Properties of Large Reinforced Concrete Members". Special Report of Institute of Technology, Shimizu Corporation, No. 25, February, 1989.
- Talbot, A.N. 1913. "Reinforced Concrete Wall Footings and Column Footings", Bulletin No.67. University of Illinois, Engineering Experiment Station, Urbana. Ill., March. 114 pp.
- Vecchio, F.J. and Collins, M.P. 1996. "Modified Compression Field Theory for Reinforced Concrete Elements Subject to Shear", ACI Structural Journal, V. 83 No.2, March-April, pp. 219-231.
- Whitney, C.S. 1957. "Ultimate Shear Strength of Reinforced Concrete Flat Slabs, Footings, Beams, and Frame Members Without Shear Reinforcement", Journal of the American Concrete Institute, V. 54, No. 4, October, pp. 265-298.

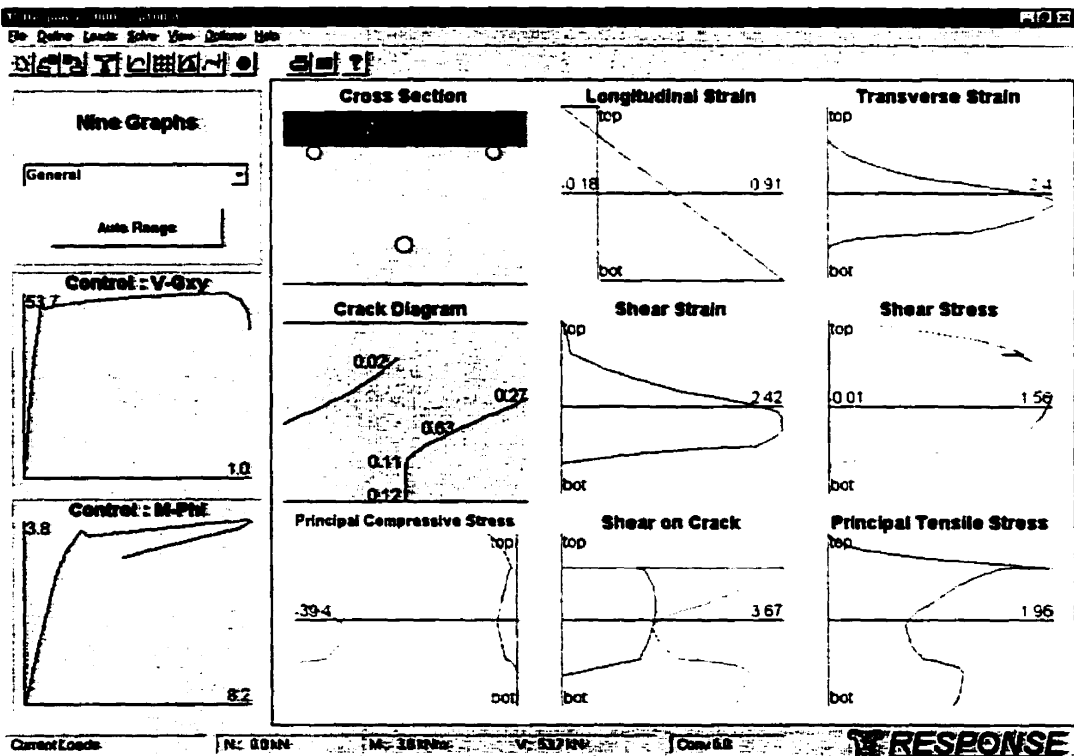
Appendix A

RESPONSE 2000[®] Input and Output

Note: The program RESPONSE 2000[®] version 1.0.0 (beta) was used.



Cross Section RESPONSE



File Edit View Options Help

Geometric Properties

	Gross Conc.	Trans (n=7.21)
Area (mm ²) × 10 ³	95.0	100.4
Inertia (mm ⁴) × 10 ⁸	385.8	306.3
r _x (mm)	95	97
r _y (mm)	95	93
S _x (mm ³) × 10 ³	3008.3	3163.7
S _y (mm ³) × 10 ³	3008.3	3286.5

Crack Spacing
 $l = d \cdot s = 0.1 \cdot d \cdot f_p$

Loading (N.M.V = gN.gM.gV)
 0.0, 0.0, 0.0 → 0.0, 0.1029, 1.0

Concrete

$f_c = 39.4 \text{ MPa}$
 $e_c = 2.09 \text{ mm/mm}$

Rebar

$f_y = 485 \text{ MPa}$
 $f_u = 698 \text{ MPa}$

All dimensions in millimetres
 Clear cover to reinforcement = 25 mm

Specimen P150 at distance d from column face
 Kevin Ka Lun Li 2000/3/6

Cross Section **RESPONSE**

File Edit View Options Help

General
 Auto Range

Control: V-Qxy
 8.9 1.1

Control: M-Phi
 8.9 5.0

Cross Section

Longitudinal Strain

Transverse Strain

Crack Diagram

Shear Strain

Shear Stress

Principal Compressive Stress

Shear on Crack

Principal Tensile Stress

Current Loads: [N: 0.01kN] [M: 0.51kNm] [V: 0.53kN] [Cont: 1.0]

RESPONSE

File Edit Load Solve View Define Help

Geometric Properties

	Gross Conc.	Trans (n=7.21)
Area (mm ²) × 10 ³	144.0	152.7
inertia (mm ⁴) × 10 ⁶	691.2	755.0
r _x (mm)	130	122
r _y (mm)	130	118
S _x (mm ³) × 10 ³	5760.0	6185.3
S _y (mm ³) × 10 ³	5760.0	6401.3

Crack Spacing
 $s = d_{cr} + 0.1 d_w / \rho$

Loading (N M V = dN dM dV)
 0.0 0.0 0.0 = 0.0, 0.1345 1.0

Concrete
 $f_c = 35.4 \text{ MPa}$
 $\epsilon_c = 2.09 \text{ mm/mm}$
 $\epsilon_{cr} = 20 \text{ mm}$
 $f_{cr} = 1.95 \text{ MPa (SL20)}$

Rebar
 $f_y = 485 \text{ MPa}$
 $f_t = 698 \text{ MPa}$
 $\epsilon_s = 100.0 \text{ mm/mm}$

All dimensions in millimetres
 Clear cover to reinforcement = 25 mm

Specimen P200 at distance d from column face
 Kevin Ka Lun Li
 2000/3/6

Cross Section RESPONSE

File Edit Load Solve View Define Help

Nine Graphs

General

Control: V-Qxy

Control: M-Phi

Current Loads: [N: -0.1 kN] [M: 12.2 kNm] [V: 12.2 kN] [Dist: 61]

Cross Section

Longitudinal Strain

Transverse Strain

Crack Diagram

Shear Strain

Shear Stress

Principal Compressive Stress

Shear on Crack

Principal Tensile Stress

Current Loads: [N: -0.1 kN] [M: 12.2 kNm] [V: 12.2 kN] [Dist: 61] RESPONSE

File Edit Load Solve View Options Help

RESPONSE

Geometric Properties		
	Gross Conc.	Trans (m=7.21)
Area (mm ²) × 10 ³	276.0	291.0
Inertia (mm ⁴) × 10 ⁸	2737.6	3015.3
y _c (mm)	172	176
y _s (mm)	172	169
S _x (mm ³) × 10 ³	15870.0	17127.5
S _y (mm ³) × 10 ³	15870.0	17847.1

Crack Spacing
 $s = \text{dist} \cdot 0.1 \cdot f_y / \rho$

Loading (N.M., V = qN, qM, qV)
 0.0, 0.0, 0.0 - 0.0, 0.1975, 1.0

Concrete

$f_c = 39.4 \text{ MPa}$

$\lambda = 20 \text{ mm}$

$f = 1.98 \text{ MPa (NACI)}$

$c_c = 2.09 \text{ mm/mm}$

Rebar

$f_y = 702 \text{ MPa}$

$f_t = 488$

$c_s = 100.0 \text{ mm/mm}$

All dimensions in millimetres
 Clear cover to reinforcement = 25 mm

Specimen P300 at distance d from column face
 Kevin Ka Lun Li 2000/3/6

Cross Section **RESPONSE**

File Edit Load Solve View Options Help

RESPONSE

Nine Graphs:

General

Auto Range

Control: V-Qxy

251.9

1.0

Control: M-PNe

45.8

2.3

Cross Section

Longitudinal Strain

top

0.11

0.14

bot

Transverse Strain

top

0.1

bot

Crack Diagram

0.09

0.05

Shear Strain

top

0.21

bot

Shear Stress

top

0.01

1.50

bot

Principal Compressive Stress

top

0.394

bot

Shear on Crack

top

3.57

bot

Principal Tensile Stress

top

1.96

bot

Current Loads: [N: 0.21M] [M: 45.81kNm] [V: 251.9kN] [Dist: 0.0]

RESPONSE

File Edit View Load Solver View Define Help
RESPONSE

Geometric Properties		
	Gross Conc	Trans (m7 21)
Area (mm ²) × 10 ³	495.0	519.5
Inertia (mm ⁴) × 10 ⁸	8353.1	9194.0
r _x (mm)	225	231
r _y (mm)	225	219
S _x (mm ³) × 10 ³	37125.0	39782.2
S _y (mm ³) × 10 ³	37125.0	42002.4

Crack Spacing

$s = d \cdot 0.1 \cdot d_b / \rho$

Loading (N, M, V = dN, dM, dV)

0.0 0.0 0.0 = 0.0 0.188 1.0

All dimensions in millimetres
Clear cover to reinforcement = 25 mm

Concrete

$f_c' = 19.4 \text{ MPa}$

Rebar

$f_y = 650 \text{ MPa}$

Specimen P400 at distance d from column face

Kevin Ka Lun Li

2000/3/6

Cross Section **RESPONSE**

File Edit View Load Solver View Define Help
RESPONSE

Nine Graphs

General

Auto Range

Control: V-Qxy

Control: M-Phi

Cross Section

Longitudinal Strain

Transverse Strain

Crack Diagram

Shear Strain

Shear Stress

Principal Compressive Stress

Shear on Crack

Principal Tensile Stress

Current Loads: N: 0.41kN, M: 92.7Nm, V: 485.9N, C: 10.0

RESPONSE

71

File Edit View Tools Windows Database Help

Geometric Properties

	Gross Conc.	Trans (n=7.21)
Area (mm ²) × 10 ³	715.0	751.9
Inertia (mm ⁴) × 10 ⁶	18024.0	30036.1
y ₁ (mm)	275	383
y ₂ (mm)	275	357
S _x (mm ³) × 10 ³	65541.7	70982.7
S _y (mm ³) × 10 ³	65541.7	74947.6

Crack Spacing
 $s = dist - 0.1 \cdot d_c / \rho$

Loading (N, M, V = dN, dM, dV)
 0.0, 0.0, 0.0 -> 3.0, 0.1563, 1.0

Concrete: $f_c' = 39.4 \text{ MPa}$, $\epsilon_c = 2.09 \text{ mm/mm}$, $s = 20 \text{ mm}$, $\epsilon = 1.98 \text{ MPa (auto)}$

Rebar: $f_y = 433 \text{ MPa}$, $\epsilon_s = 100.0 \text{ mm/mm}$

— A_s = 1000 mm²
 — A_s = 4937 mm²

All dimensions in millimetres
 Clear cover to reinforcement = 25 mm

Specimen P500 at distance d from column face
 Kevin Ka Lun Li 2000/3/6

Cross Section: RESPONSE

File Edit View Tools Windows Database Help

File Edit View Tools Windows Database Help

Nine Graphs

General Auto Range

Control: V-Qxy

Control: V-Qx

Cross Section

Crack Diagram

Longitudinal Strain

Transverse Strain

Shear Strain

Shear Stress

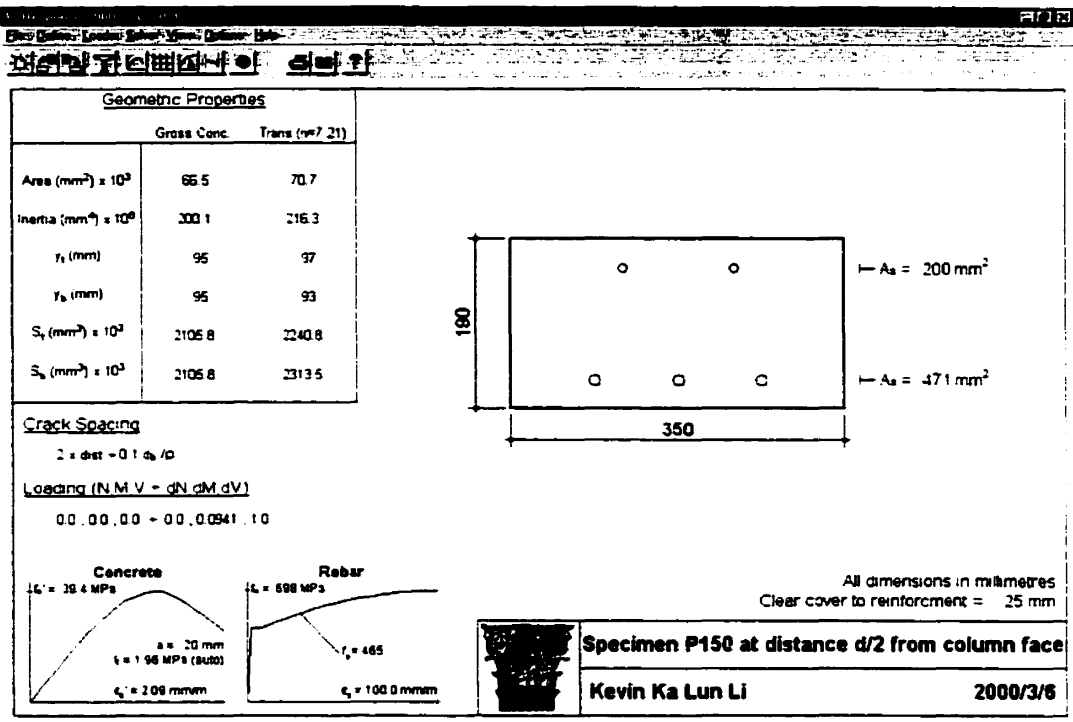
Principal Compressive Stress

Shear on Crack

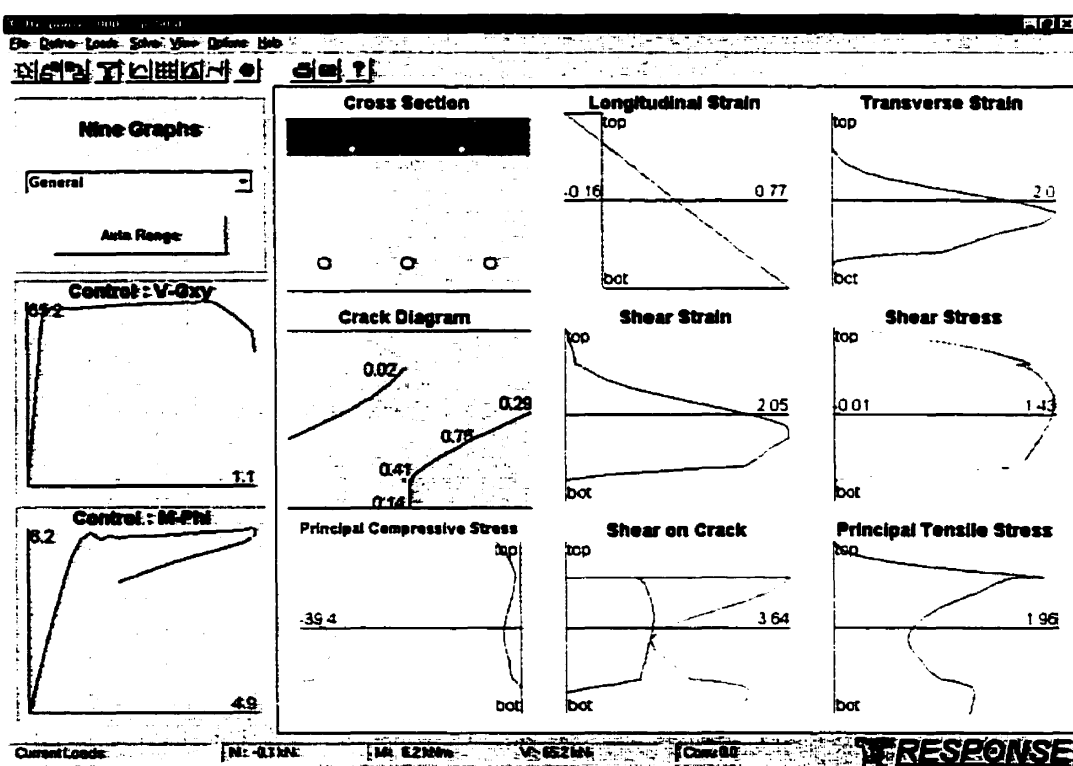
Principal Tensile Stress

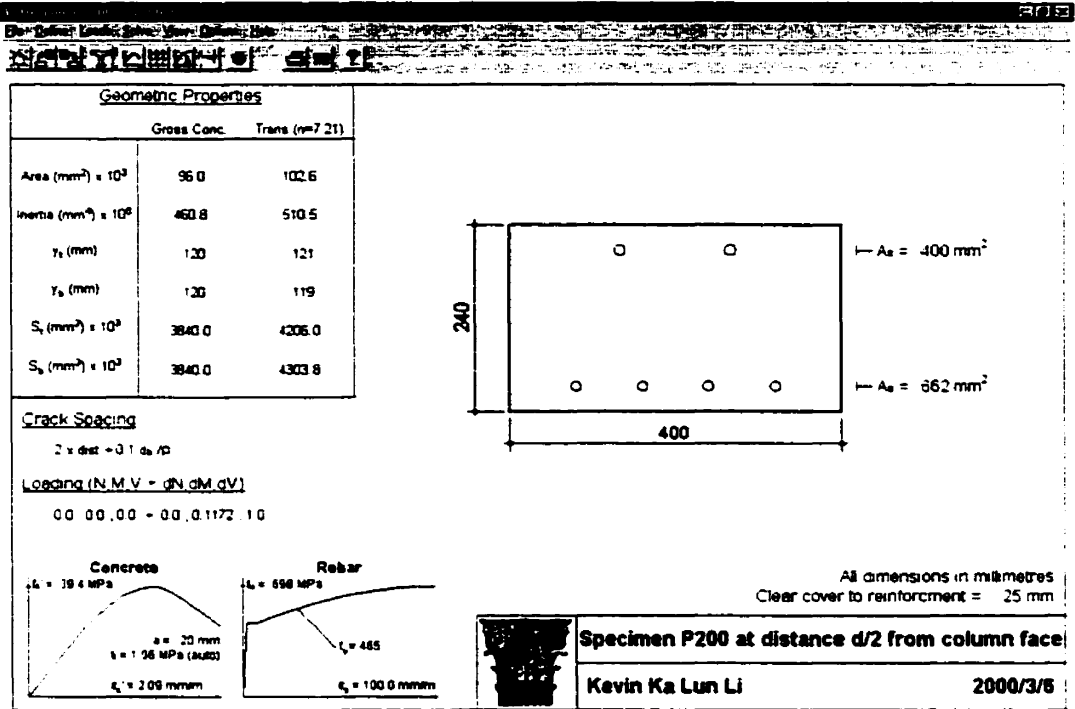
Current Loads: N: 0.010t | M: 135.41kNm | V: 988.61kN | Control

RESPONSE

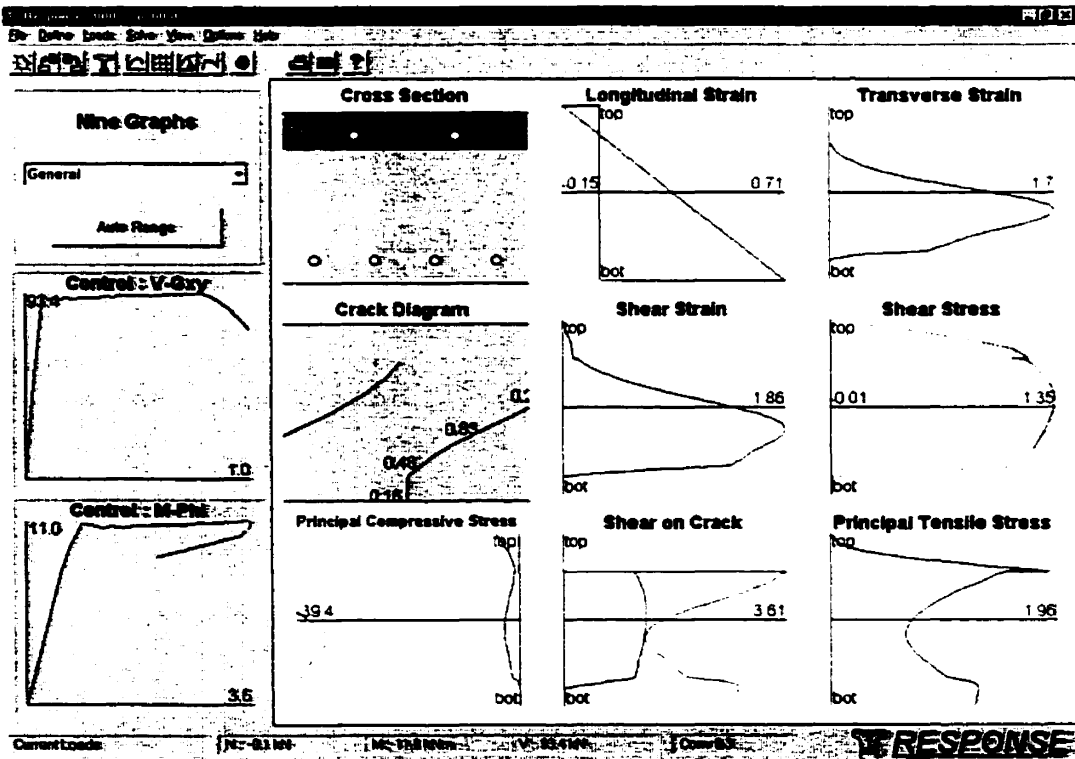


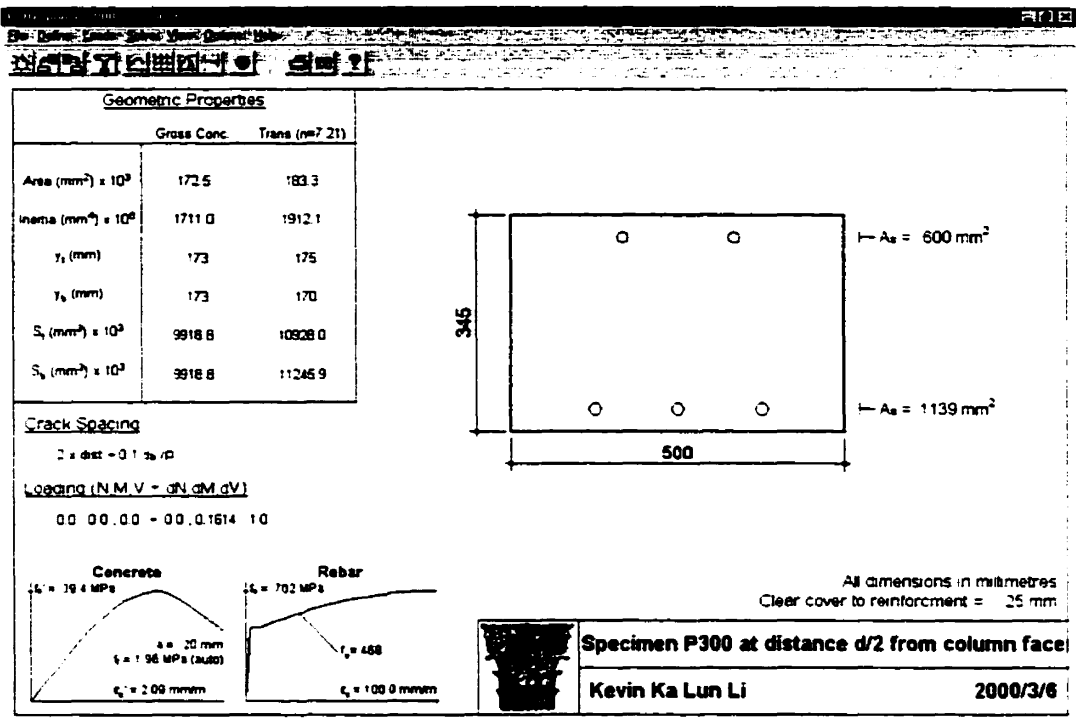
Cross Section **RESPONSE**



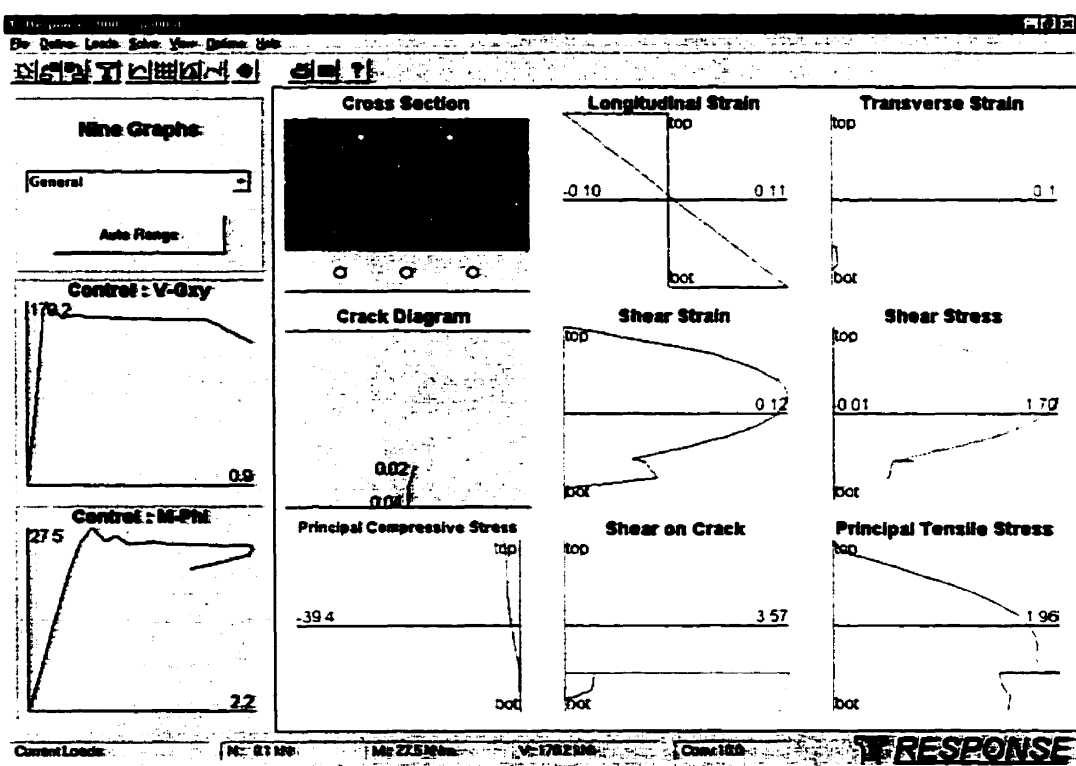


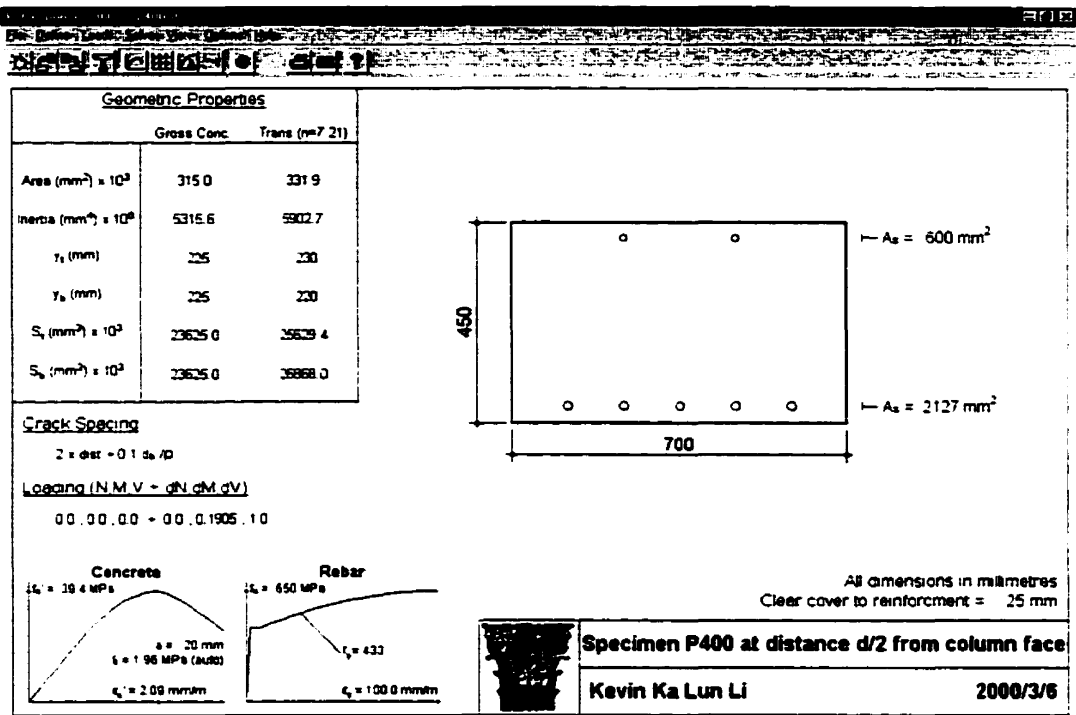
Cross Section: RESPONSE



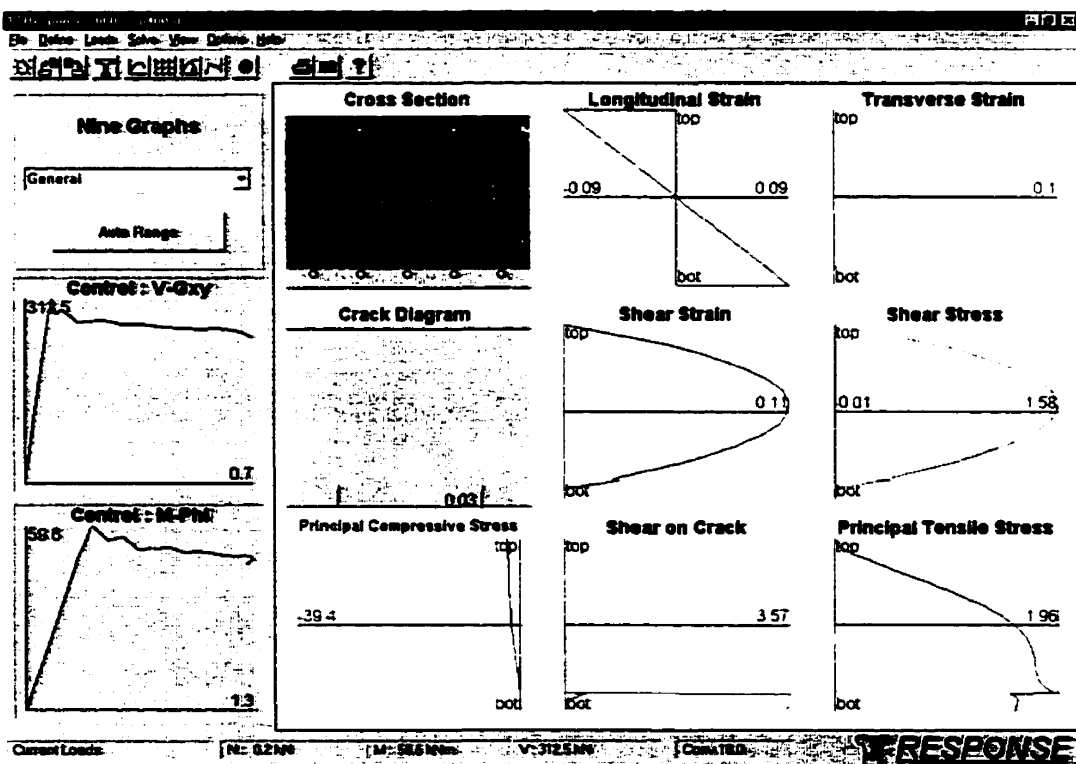


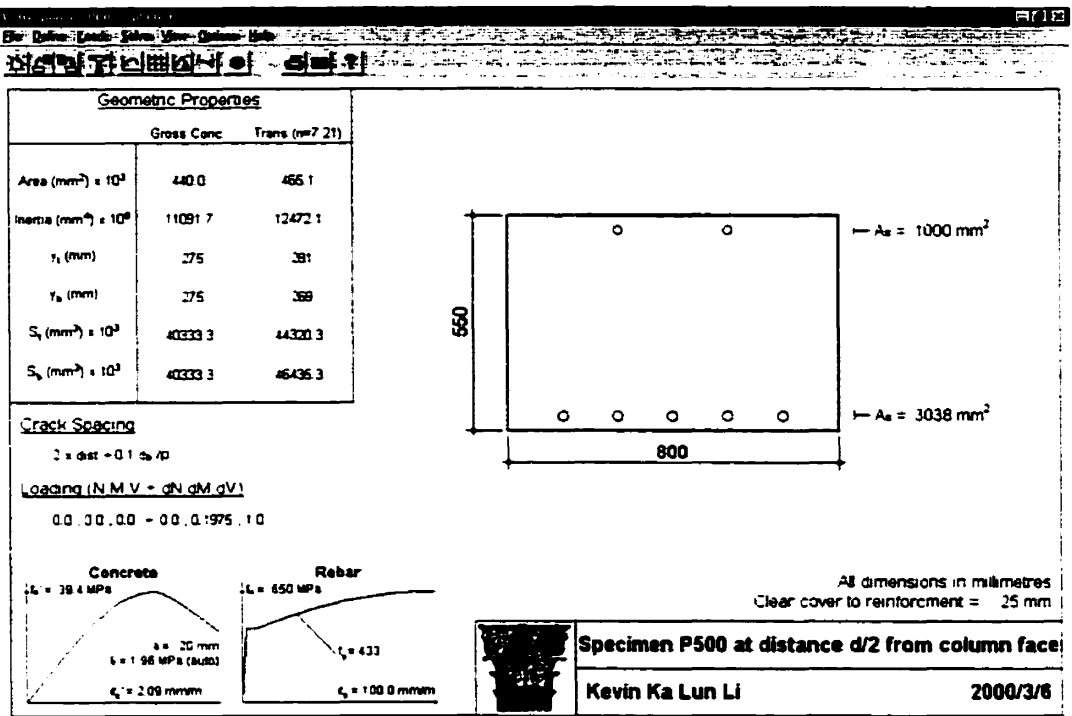
Cross Section **RESPONSE**





Current Loads: [N: 0.2 kN] [M: 58.6 Nm] [V: 312.5 kN] [Cov: 100] **RESPONSE**





Cross Section RESPONSE

